

A taste of dark portals

Flavour constraints on vectorial dark matter from rare meson decays

Master's thesis in Master of Physics

EMIL ÅSTRAND

DEPARTMENT OF PHYSICS

CHALMERS UNIVERSITY OF TECHNOLOGY
Gothenburg, Sweden 2021
www.chalmers.se

MASTER'S THESIS 2021

A taste of dark portals

Flavour constraints on vectorial dark matter from rare meson decays

EMIL ÅSTRAND



CHALMERS
UNIVERSITY OF TECHNOLOGY

Department of Physics
Division of Subatomic, High Energy and Plasma Physics
CHALMERS UNIVERSITY OF TECHNOLOGY
Gothenburg, Sweden 2021

A taste of dark portals
Flavour constraints on vectorial dark matter from rare meson decays
EMIL ÅSTRAND

© EMIL ÅSTRAND, 2021.

Supervisor: Riccardo Catena, Department of Physics
Examiner: Andreas Martin Heinz, Department of Physics

Master's Thesis 2021
Department of Physics
Division of Subatomic, High Energy and Plasma Physics
Chalmers University of Technology
SE-412 96 Gothenburg
Telephone +46 31 772 1000

Cover: The original electroweak penguin diagram for $b \rightarrow s$ decay. Original image credit: Nico Serra and Tom Blake [1].

Typeset in L^AT_EX
Printed by Chalmers Reproservice
Gothenburg, Sweden 2021

A taste of dark portals
Flavour constraints on vectorial dark matter from rare meson decays
EMIL ÅSTRAND
Department of Physics
Chalmers University of Technology

Abstract

Overwhelming evidence on all cosmological scales points to the inevitable existence of Dark Matter (DM), constituting approximately 85% of all matter in the Universe. The different evidence have one thing in common: they all depend on indirect, gravitational effects arising from the presence of DM. The particle nature of DM remains unknown.

While the Weakly Interacting Massive Particle (WIMP) has been a promising candidate to DM, extensive direct detection searches has not yet found a conclusive signal. A possibility is that DM does not interact directly with the Standard Model (SM) but rather through an unstable mediator particle, scenarios commonly referred to as dark portals. A way to probe such models is through flavour changing rare decays of mesons, which are heavily suppressed in the SM, but receive contributions from dark portal models.

In this work I consider a model where spin-1 DM is realised as a hidden $U(1)$ symmetry, spontaneously broken by a singlet scalar that acts as the mediator and mixes with the SM Higgs field. This extension induces contributions to the branching fractions $B_{s,d}^0 \rightarrow \ell^+ \ell^-$ where the particular ones $B_s^0 \rightarrow \mu^+ \mu^-$ and $B^0 \rightarrow \mu^+ \mu^-$ have been measured experimentally. The contributions were found to be primarily dependent on the mixing angle α and the mediator mass M_{H_1} . I find that while the most likely combination of fundamental parameters lies on the straight line $\sin^2 \alpha / M_{H_1}^2 = 0.001$ where $\sin \alpha \in [10^{-3}, 1]$ and $M_{H_1} \in [10^{0.5}, 10^{1.5}]$ GeV, a large region below this line possess a flat, intermediate likelihood. This is due to the effects of H_1 's presence is heavily suppressed by its mass.

At the moment the analysis of constraints on spin-1 DM by rare meson decays is largely unexplored in literature. This thesis provides first steps towards filling this gap.

Keywords: dark matter, flavour physics, B-meson, higgs portal, rare decays.

Acknowledgements

Thank you Riccardo Catena, for all your support during not only this masters thesis but also during my bachelors thesis and the publication that it led to. It has been a pleasure working with you, and I sincerely hope we will in the future. Thank you Alex Bökmark, for all the rewarding discussions and for helping me keep sane during this pandemic. We should tear our hair out together in real life next time. A special thanks to Mikael Öhman at C3SE for his aid when building code on the Vera cluster. Thank you all my friends and family that have supported me, no matter what. Especially thanks to you, Kristin. And to my dog Lilo, forcing me to take breaks by biting me real hard.

Emil Åstrand, Gothenburg, June 2021

Contents

List of Figures	xi
List of Tables	xiii
1 Introduction	1
1.1 Aim	2
1.2 Outline	2
2 Background	3
2.1 Evidence for dark matter	3
2.1.1 Galactic rotation curves	3
2.1.2 Gravitational lensing	5
2.1.3 CMBR anisotropies	5
2.2 Experimental searches	7
2.2.1 Direct detection	8
2.2.2 Indirect detection	8
2.2.3 Particle colliders	9
2.3 Decays of rare mesons	9
3 Theory	11
3.1 Vectorial dark matter model	11
3.1.1 A hidden $U(1)_X$ symmetry	11
3.1.2 The Higgs portal	13
3.2 Flavour physics	15
3.2.1 Operator product expansion in weak decays	16
3.2.2 The standard operator basis	17
3.2.3 Computation of Wilson coefficients and renormalization group equations	19
3.2.4 Flavour changing transitions	20
4 Computational tools	23
4.1 GAMBIT	23
4.1.1 FlavBit	24
4.2 SARAH/FlavorKit	26
4.2.1 VDM.m	27
4.2.2 particles.m	28
4.2.3 parameters.m	30

4.2.4	SPheno.m	31
4.3	SPheno	33
4.4	wilson	34
4.5	Performed GAMBIT runs	34
5	Results	37
5.1	Branching fractions	37
5.2	Likelihoods	40
6	Conclusions	43
6.1	Future work	44
	Bibliography	45
A	Mathematical derivations	I
A.1	Kinetic term $(D_\mu S)^\dagger(D^\mu S)$	I
A.2	Tadpole equations	I
A.3	Mass matrix	II
A.4	Parameter substitutions	II
B	Computer cluster setups	V
B.1	Vera	V
B.2	Tetralith	VI
C	Source code	IX
C.1	SARAH	IX
C.1.1	VDM.m	IX
C.1.2	parameters.m	XI
C.1.3	particles.m	XIV
C.1.4	SPheno.m	XVII
C.2	translate.py	XVIII
C.3	GAMBIT	XIX
C.3.1	WCVectorDM.hpp	XX
C.3.2	WCVectorDM.cpp	XX
C.3.3	LLrun.yaml	XXX

List of Figures

2.1	HI surface density (left) and rotation curve (right) as functions of galactic radius, for five different galaxies as observed by Rogstad and Shostak [2]. The bars under each galaxy name corresponds to average radial beam diameters, and R_{80} is the radius within 80 % of the observed HI is found.	4
2.2	The Abell 370 galaxy cluster and its great arc, seen in the right. This arc is the distorted image due to gravitational lensing of a source behind the cluster. Credit: NASA, ESA, the Hubble SM4 ERO Team, and ST-ECF.	6
2.3	The angular power spectrum measured by WMAP, shown as red dots with error bars. On the vertical axis, $\mathcal{D}_\ell = \ell(\ell + 1)C_\ell/(2\pi)$ is plotted against the multipole moment (lower axis) and angular scale (upper axis). The solid curve shows the best fit for a Λ CDM model, indicating uncertainties with a shaded band. Credit: The Planck Collaboration, acquired from reference [3].	7
2.4	An overview of the searches for $B_s^0 \rightarrow \mu^+\mu^-$ (blue) and $B^0 \rightarrow \mu^+\mu^-$ (red) as reported by 11 experiments spanning over more than 30 years. SM predictions are shown as lines, while experimental measurements are reported as markers with error bars denoting 68 % confidence intervals. Markers without error bars correspond to upper limits at 90 % confidence levels. Image acquired from reference [4].	10
3.1	Examples of penguin (left) and box (right) diagrams for FCNC transitions related to the decay of $B_s^0 \rightarrow \ell^+\ell^-$. Here, $q = u, c, t$	16
5.1	Branching fraction of the decay $B_s^0 \rightarrow \mu^+\mu^-$ as a function of the additional Higgs-like boson mass M_{H_1} in the dark portal model, for three distinct values of the sine of the mixing angle $\sin \alpha = 0.001, 0.01, 0.1$ (blue, orange, green). The Standard Model prediction (red) and experimental measurements (magenta) are presented for comparison. Uncertainties for the experimental value are given in table 2.1.	38
5.2	Branching fraction of the decay $B^0 \rightarrow \mu^+\mu^-$ as a function of the additional Higgs-like boson mass M_{H_1} in the dark portal model, for three distinct values of the sine of the mixing angle $\sin \alpha = 0.001, 0.01, 0.1$ (blue, orange, green). The Standard Model prediction (red) and experimental measurements (magenta) are presented for comparison. Uncertainties for the experimental value are given in table 2.1.	38

5.3	Branching fraction of the decay $B_s^0 \rightarrow e^+e^-$ as a function of the additional Higgs-like boson mass M_{H_1} in the dark portal model, for three distinct values of the sine of the mixing angle $\sin \alpha = 0.001, 0.01, 0.1$ (blue, orange, green). The Standard Model prediction (red) is presented for comparison.	39
5.4	Surface plot of the combined likelihoods from branching fractions $\mathcal{B}(B_s^0 \rightarrow \mu^+\mu^-)$ and $\mathcal{B}(B^0 \rightarrow \mu^+\mu^-)$. The fundamental parameters $\sin \alpha$ and M_{H_1} were varied using the Diver scanner in GAMBIT. The white lines indicate the 68.3 % confidence level. Plots were obtained using Pippi [5].	41
5.5	Surface plot of the combined likelihoods from branching fractions $\mathcal{B}(B_s^0 \rightarrow \mu^+\mu^-)$ and $\mathcal{B}(B^0 \rightarrow \mu^+\mu^-)$. The fundamental parameters $\sin \alpha$ and M_{H_1} were varied using the MultiNest scanner in GAMBIT. The white lines indicate the 68.3 % confidence level. Plots were obtained using Pippi [5].	42

List of Tables

2.1	Experimental status of B-meson decays into lepton pairs. The upper limits on decays to e^+e^- were determined at 90% Confidence Level (CL) and decays to $\tau^+\tau^-$ were determined at 95% CL [6]. The first uncertainty in the decays to $\mu^+\mu^-$ refers to statistical uncertainties, while the second refers to systematic uncertainties.	10
4.1	Values for the different scans. In the different samplers, points refer to population density (N_P), live points (N_{live}) and evenly spaced grids (N). See text for explanation. For all runs, the branching fractions of the decays $B_0^s \rightarrow \mu^+\mu^-$, $B^0 \rightarrow \mu^+\mu^-$ and $B_s^0 \rightarrow e^+e^-$ were computed.	35

1

Introduction

Originally a hyperonym of unobservable celestial phenomena such as dark planets, stars, or clouds [7], Dark Matter (DM) is today established as collections of particles that do not interact electromagnetically, at any wavelength. Rather, it only affects matter and photons surrounding it via gravitational effects. Despite such limited interactions, overwhelming evidence on all cosmological scales points to the existence of DM. Created in the early Universe, it impacted the large scale structure formation by affecting the gravitational wells where ordinary matter clustered and formed galaxies, manifested through anisotropies in the Cosmic Microwave Background (CMB) radiation. It envelops galaxies in large halos. It bends light itself around galaxy clusters.

While numerous particle candidates for dark matter have been proposed as the solution, only a few have persisted and are now considered paradigm. The Weakly Interacting Massive Particle (WIMP) is one of the most prosperous models. In recent years, extensive searches hunting for any sign of the WIMP has been carried out. While these experiments have set tremendous constraints on the allowed parameter space for the WIMP, the elusive particle is yet to be found. These constraints have in turn made it difficult to reconcile current observations with a direct coupling between DM and the Standard Model (SM) particles [8].

A possible remedy to this situation is to postulate the existence of additional particles, which together with the DM particle constitutes what is commonly referred to as the dark sector. This sector might be constructed in such a way that the DM only interacts with the SM via one, or several mediator particles. Such scenarios are often called portals, where DM is in a sense detached from the SM so that constraints from experiments could better be placed on the mediator particle instead of on the DM particle.

If the mediator in the considered portal model is light, flavour-changing neutral processes occurring at the one-loop level or higher could receive substantial contributions and therefore present a unique way of constraining such models.

In this thesis, I set constraints on the popular dark portal named the Higgs portal probed via its influence on the flavour-changing neutral processes that occur in weak decays of rare mesons. As will be explained in detail below, in the Higgs portal scenario a spin-1 DM boson arises from an additional $U(1)$ gauge symmetry, spontaneously broken by a scalar particle that mediates interactions between the

SM and DM through mixings in the Higgs sector.

1.1 Aim

The thesis main aim is to set constraints on the fundamental parameters in the Higgs portal scenario, probed via weak decays of B -mesons into electron- or muon pairs. The fundamental parameters include the mediator mass M_{H_1} , the DM mass M_V , the dark $U(1)$ gauge coupling g_X and the sine of the mixing angle $\sin\alpha$ that quantifies the strength of the mass mixing in the Higgs sector.

1.2 Outline

The thesis begins with a chapter aimed to provide the reader with the relevant background needed to follow the rest of the thesis. In this chapter I describe some of the primary and most studied evidence for DM, the experimental searches in the context of the WIMP conducted in recent years, concluding by describing current experimental bounds and measurements in the context of rare meson decays.

Continuing, the theory chapter is separated in two parts. In the first part, the model under investigation, i.e. the Higgs portal, is described together with the free fundamental parameters of this theory. In the second part, I describe how to bring the model from the full theory to an effective theory, and how to probe the interactions via rare meson decays.

A review of the computational tools used follows, starting with an overview of the full implementation. This implementation is then broken down into parts, where I describe in detail each part of this computational framework. I conclude this chapter with an overview of the performed computations. The results are then presented and discussed, followed by my conclusions and suggestions for further development.

2

Background

Dark matter has an incredibly rich history, puzzling the scientific community increasingly during the last century. I summarise this history rather crudely by presenting three observations that played an important part in bringing undeniable evidence towards the existence for DM throughout these years. I continue by giving a brief review on the experimental searches, in the WIMP context, that has been conducted extensively for the last decade. The last section is meant to give an overview of the experimental history and status for rare meson decays, specifically the mode where $B_{d,s}^0$ decays into lepton pairs.

2.1 Evidence for dark matter

What makes the evidence for DM so overwhelming is not just that there are plenty, but also that it exist on all cosmological scales, from the galactic scale to being evident from the Cosmic Microwave Background (CMB), i.e. the scale of the Universe and how it can be traced back to structure formation in the early Universe. I will therefore start on the "smaller" galactic scale, going forward to the medium scale of galaxy clusters, and end on the large scale, essentially the scale of the causally connected Universe.

2.1.1 Galactic rotation curves

The discrepancy between the waning of mass in outskirts of galaxies and the velocity which the mass rotates around the galaxy with became clear as early as 1939 by Horace Babcock, but it was not until the 1970s when observational quality had been improved enough that studies of this subject exploded [7]. It was also at this time the discrepancy was explained through some "missing mass" at the edges of galaxies. Comparisons of 21 cm observations of neutral atomic hydrogen (HI) gas in five different galaxies and their respective rotation curves was performed by Rogstad and Shostak in 1972 [2] where they found the galactic rotation curves flattened out while the visible gas mass decreased, see figure 2.1 for their results. The rotational velocity is given by [9]

$$V^2(R) = \frac{GM(R)}{R} \quad (2.1)$$

where R is the distance from the galactic center, G Newton's gravitational constant and $M(R)$ the mass contained within a sphere of radius R . The rotational velocity is expected to decrease if the mass decreases, or if the radius increase. Furthermore,

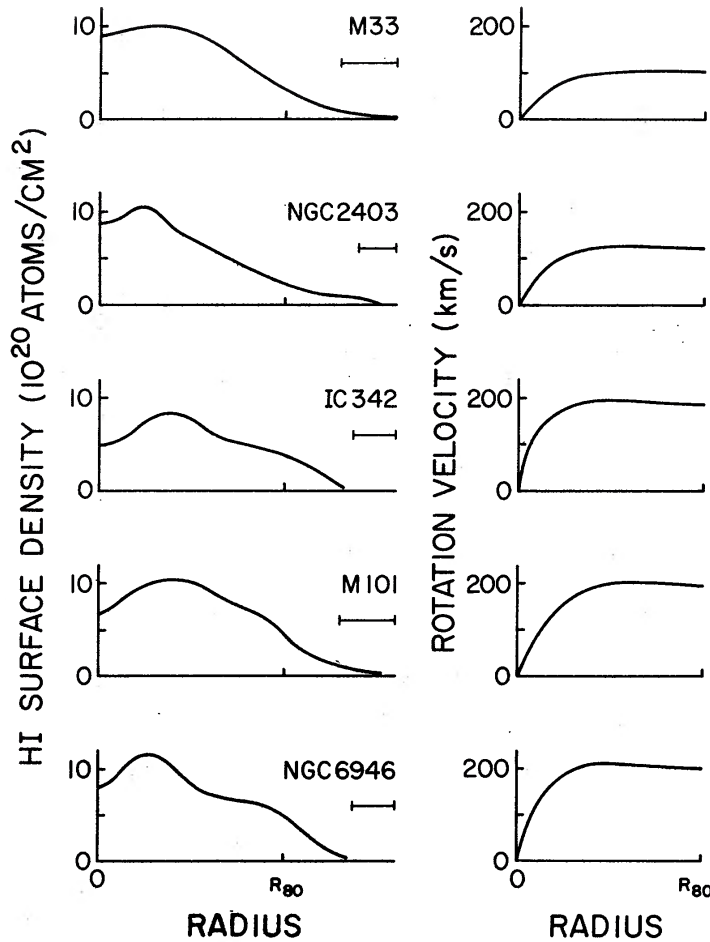


Figure 2.1: HI surface density (left) and rotation curve (right) as functions of galactic radius, for five different galaxies as observed by Rogstad and Shostak [2]. The bars under each galaxy name corresponds to average radial beam diameters, and R_{80} is the radius within 80 % of the observed HI is found.

$M(R)$ is given by

$$M(R) = 4\pi \int_0^R \rho(r) r^2 dr \quad (2.2)$$

so that by modifying the density profile $\rho(r)$ the DM can be accounted for. Usually, the DM in outskirts of galaxies is depicted as a halo engulfing the galaxy. A very common density profile used when modeling DM halos is the Navarro-Frenk-White (NFW) profile [10],

$$\rho(r) = \frac{\rho_s}{(r/r_s)(1 + r/r_s)^2} \quad (2.3)$$

where r_s is a characteristic radius and ρ_s determines the amplitude of the profile, both parameters varying depending on the halo model. Using this profile, $M(R)$ is solved as

$$M(R) = 4\pi\rho_s R^3 \left[\ln \left(\frac{r_s + R}{r_s} \right) + \frac{r_s}{r_s + R} - 1 \right]. \quad (2.4)$$

Indeed, the DM halo starts at $r = 0$ and extends up to the virial radius ~ 200 kpc. From (2.3), note that for $r \gg r_s$, $\rho(r) \sim r^{-3}$ whereas for $r \ll r_s$, $\rho(r) \sim r^{-1}$. Therefore, around $r = r_s$ the DM profile changes slope.

2.1.2 Gravitational lensing

A famous result of Einstein's theory of general relativity is that densely concentrated masses such as galaxy cores or galaxy clusters have such a strong gravitational force that they have the ability to warp space-time around them [11]. In doing so, light can travel on multiple paths around the object and still be deflected towards the observer. The massive object is said to act as a lens. Although very rare, sources may appear directly behind the lens in the line of sight and then create an Einstein ring around the lens, with a radius proportional to the lensing objects mass [11]. The first observation of such an event was during a solar eclipse in front of the Hyades star cluster, whose stars seemed to move as they passed behind the sun [11]. It is one of the most direct methods to study the influence of dark matter present in the Universe.

The first image of a strongly lensed arc was obtained with the Canada-France Hawaii telescope in 1987 in the galaxy cluster Abell 370 [12, 13] and was confirmed to originate from a single source almost twice as far away as the cluster. A more recent image of the arc was taken by the Hubble Space Telescope (HST), see figure 2.2.

Strong gravitational lenses are rare. For most lenses, the deflection is very slight and in the so called weak lensing regime. In this regime, the signal is rather a distortion in the background galaxy by the curvature of the foreground gravitational potential. This implies that even though there is no visible mass to distort the background, the distortion could be inferred by a foreground composed of dark matter [14]. Hence, mapping the distortions and inverting them sheds light on the large scale structure of dark matter in the Universe. Gravitational lensing is hence not just a direct verification of dark matter, but may also be used as a tool for tracing its distribution.

2.1.3 CMBR anisotropies

The arguably most important observation in cosmology is the Cosmic Microwave Background (CMB), an echo of the big bang and a remnant from the time in the early Universe when photons and matter decoupled. It has a spectrum resembling a perfect blackbody, filling the Universe in every direction. First observations by the Cosmic Microwave Background Explorer (COBE) found tiny anisotropies in this almost homogenous radiation field. Greater resolution of the CMB was obtained by Wilkinson Microwave Anisotropy Probe (WMAP) and was further improved by the Planck satellite, measuring the anisotropies to the scale 10^{-5} . The explanation of these temperature anisotropies is that before the matter-radiation decoupling, the Universe can be modelled as a photon-matter fluid that goes through a cycle. The fluid is compressed as it falls into a gravitational well, its pressure continues to in-



Figure 2.2: The Abell 370 galaxy cluster and its great arc, seen in the right. This arc is the distorted image due to gravitational lensing of a source behind the cluster. Credit: NASA, ESA, the Hubble SM4 ERO Team, and ST-ECF.

crease until it forces the fluid to expand outward, making the pressure decrease as it expands until gravity pulls it back [15]. The cycle is broken once the photons decouple, and those that emerge vary in temperature. The observed fluctuations are hence disturbances in the primordial density, dependent on the matter content at this time in the early Universe.

The temperature fluctuations of the CMB are seen as projections in a 2D spherical surface sky and so the temperature field is usually expanded using spherical harmonics, which form a complete orthonormal set on the unit sphere and are defined as [16]

$$Y_{\ell m} = \sqrt{\frac{2\ell + 1}{4\pi} \frac{(\ell - m)!}{(\ell + m)!}} P_{\ell}^m(\cos \theta) e^{im\phi} \quad (2.5)$$

where $\ell = 0, \dots, \infty$, $-\ell \leq m \leq \ell$ and P_{ℓ}^m are the Legendre polynomials. The multipole ℓ represent an angular scale in the sky given approximately by $\alpha = 180/\ell$ in degrees. Expanding the fluctuation field, a power spectrum can be obtained where anisotropies are quantified by the multipole coefficients C_{ℓ} , dependent on the above

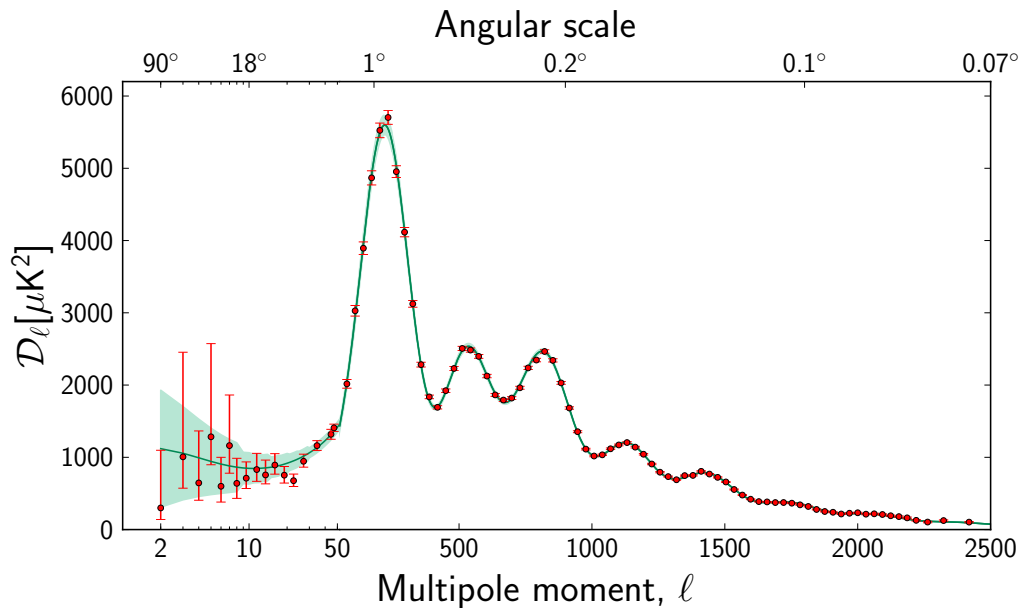


Figure 2.3: The angular power spectrum measured by WMAP, shown as red dots with error bars. On the vertical axis, $\mathcal{D}_\ell = \ell(\ell + 1)C_\ell/(2\pi)$ is plotted against the multipole moment (lower axis) and angular scale (upper axis). The solid curve shows the best fit for a Λ CDM model, indicating uncertainties with a shaded band. Credit: The Planck Collaboration, acquired from reference [3].

mentioned spherical harmonics [9].

Analysis of the WMAP data recovered such power spectrum plots, dependent on ℓ . A prediction of the power spectrum can also be obtained from theoretical models. The Planck Collaboration fitted the resulting anisotropies power spectrum with a spatially-flat six parameter Λ CDM (Cold dark matter with Einsteins cosmological constant) model and found that such a model describes the data extremely well, see figure 2.3 for their results and fit. They found that the densities of baryons, cold dark matter, and total matter are [17]

$$\Omega_b h^2 = 0.02205 \pm 0.00028, \quad \Omega_c h^2 = 0.1199 \pm 0.0027, \quad \Omega_m h^2 = 0.1426 \pm 0.0025$$

These results imply that $\Omega_c/\Omega_m \approx 0.84$ i.e. that 84 % of the matter in the Universe is dark, and was present already in its earliest days.

2.2 Experimental searches

Different techniques have been adopted searching for the WIMP candidate to DM; Direct detection, indirect detection, and production using particle colliders. While this thesis aims to explore the possibilities of portal scenarios which are different to the WIMP scenario, a review of the current search is in order since these techniques have dominated the search initiatives for the last years.

2.2.1 Direct detection

The idea of a DM halo surrounding our Galaxy, as is evident by measurements of galactic rotation curves, leads to the reasonable assumption that the Earth is constantly bombarded by DM particles. It is therefore motivated to search for signals of DM scattering off of nuclei in detectors, which is the main aim of direct detection experiments.

Even though detectors are usually seated in deep underground laboratories, shielded from e.g. cosmic rays, background can still be present in the form of e.g. detector radiation and has to be discriminated from the signal. In combination with the exposure, these determine the overall sensitivity of such experiments. Further determining factors of the sensitivity are the energy threshold and target material, that drives the sensitivity to the WIMP mass and scattering cross section [18].

The current status of the many experiments involved in the effort of direct detection is that although strong constraints have been placed on the scattering cross section and WIMP mass, no conclusive signal has yet been found. In fact, the bounds are closing in on the neutrino floor, where irreducible background from coherent neutrino-nucleus scattering take place [19]. This floor is usually taken as the WIMP detection limit. Probing down to this neutrino floor requires extremely high exposure, which is the goal of future experiments [19].

2.2.2 Indirect detection

Indirect detection relies on the possibility that annihilating pairs of DM or the respective decay of DM could produce an observable flux of gamma rays, cosmic rays, or neutrinos [18, 20]. In contrast to direct detection experiments, where the scattering of actual DM particles are measured, the remnants of DM interactions are observed in indirect experiments.

Since the annihilation, or decay of DM is proportional to the DM density, suitable targets are cosmological objects known to contain large amounts of DM. For example, dwarf spheroidal galaxies have high mass-to-light ratios with little interstellar gas, and therefore seem to be dominated by DM making them great candidates for indirect searches. Due to a lack of background of high-energy neutrinos, γ -rays or cosmic rays they present rather clean targets [20].

The indirect search initiative has reported constraints and exclusion limits that span several orders of magnitude in the WIMP mass, but as with the direct detection effort a conclusive signal is yet to be found [20]. The sensitivity aim of future experiments is to further probe smaller annihilation cross sections. An example is the upcoming Hyper-Kamiokande, aiming to probe sub-GeV WIMPs annihilating into neutrinos originating from the Galactic centre [21], another source known to hold high DM density.

2.2.3 Particle colliders

Collider searches aim to detect signatures of DM particles as byproducts produced by SM particle collisions. These searches could either probe the possibility of invisible DM particles or particles that mediate the interaction between DM and the SM, referred to as mediator particles [22]. One of the main collider searches takes place at the Large Hadron Collider (LHC) where the searches can be divided into three categories: final states with DM, without DM in the final states, and light dark matter signals from dark sectors.

The first category in which final states with DM occur are referred to as Mono-X searches [22], arising when the DM mass is small compared to the mediator, and the WIMP pair is then boosted opposite to the direction of the visible particle and leads to a Mono-X signature. Situations where DM is absent in the final state can be probed by looking at distortions in the di-jet invariant mass spectrum and/or angular corrections [22].

Searches for dark matter signals from dark sectors can be done by probing decays of intermediate states and how they change over the expected SM background. The LHC has performed measurements for e.g. Higgs decaying into intermediate states that subsequently decay into leptons, where the intermediate states could be the proposed mediator particles such as the dark photon [23, 24, 25].

2.3 Decays of rare mesons

The presence of a mediator particle can also manifest itself by changing other types of decay modes, and not only the Higgs channel. Rare decays of B -mesons for example are very sensitive to contributions from new physics, as will be clear in future chapters and the novelty of my thesis is to obtain a method for placing constraints on the Higgs portal model for DM using rare meson decay data. Thus, I will end this chapter by giving a brief history and overview of the experimental status for the particular rare decays used in this thesis.

The search for rare meson decay modes $B_{s,d}^0 \rightarrow \ell^+ \ell^-$ started in the 1980s with the CLEO, ARGUS and UA1 experiments and continued at the B -factories Belle and BaBar [4]. With the passing of time, more experiments joined the search but no evidence of the decays was found although upper limits were obtained. The LHC joined the hunt 2010 [4], focusing on the decay modes to muon pairs. The Large Hadron Collider beauty (LHCb) experiment reported its first observation of the decay $B_s^0 \rightarrow \mu^+ \mu^-$ in 2012, and in 2015 a combined analysis of the Compact Muon Solenoid (CMS) experiment and LHCb was published in Nature [26] stating the first results of the branching fractions $\mathcal{B}(B_s^0 \rightarrow \mu^+ \mu^-)$ and $\mathcal{B}(B^0 \rightarrow \mu^+ \mu^-)$. In its second run, LHCb obtained the first observation of this decay channel by a single experiment. An overview of this history is presented in figure 2.4.

While a signal for the the decay mode to muon pairs has been established, no signal

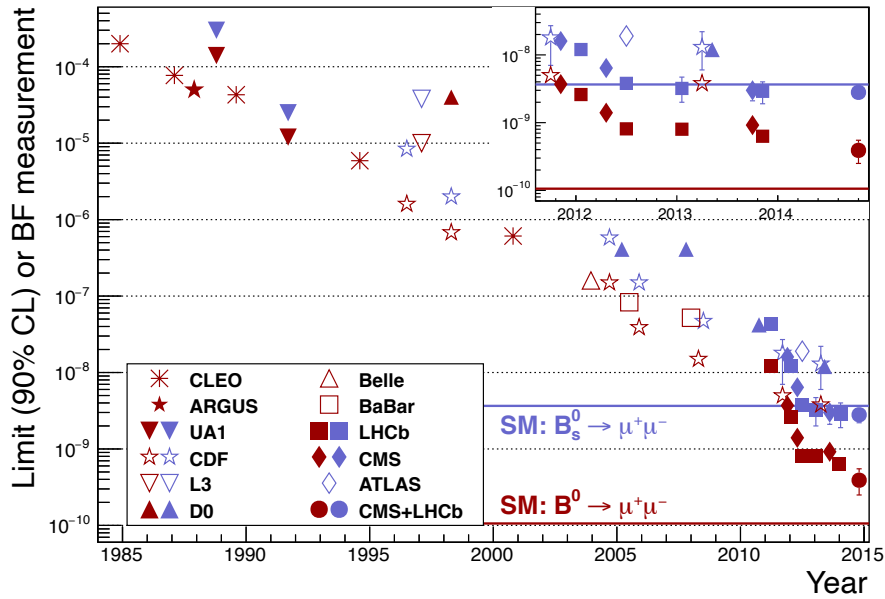


Figure 2.4: An overview of the searches for $B_s^0 \rightarrow \mu^+\mu^-$ (blue) and $B^0 \rightarrow \mu^+\mu^-$ (red) as reported by 11 experiments spanning over more than 30 years. SM predictions are shown as lines, while experimental measurements are reported as markers with error bars denoting 68 % confidence intervals. Markers without error bars correspond to upper limits at 90 % confidence levels. Image acquired from reference [4].

	e^+e^-	$\mu^+\mu^-$	$\tau^+\tau^-$
B_d^0	$< 8.3 \times 10^{-8}$ [6]	$(3.9 \pm 1.5) \times 10^{-10}$ [26]	$< 2.1 \times 10^{-3}$ [6]
B_s^0	$< 2.8 \times 10^{-7}$ [6]	$(3.0 \pm 0.6_{-0.2}^{+0.3}) \times 10^{-9}$ [29]	$< 6.8 \times 10^{-3}$ [6]

Table 2.1: Experimental status of B-meson decays into lepton pairs. The upper limits on decays to e^+e^- were determined at 90% Confidence Level (CL) and decays to $\tau^+\tau^-$ were determined at 95% CL [6]. The first uncertainty in the decays to $\mu^+\mu^-$ refers to statistical uncertainties, while the second refers to systematic uncertainties.

has been found for the decays $B_{s,d}^0 \rightarrow e^+e^-$ or $B_{s,d}^0 \rightarrow \tau^+\tau^-$. Upper limits has however been obtained, as reported by the Collider Detector at Fermilab (CDF) for the decay $B_{s,d}^0 \rightarrow e^+e^-$ [27] and by LHCb for the decay $B_{s,d}^0 \rightarrow \tau^+\tau^-$ [28]. The current measurements and upper limits are presented in table 2.1.

Being the best measured branching fraction with the smallest error bars, $\mathcal{B}(B_s^0 \rightarrow \mu^+\mu^-)$ constitutes a 'golden channel' in the search for physics beyond the standard model [4] due to its sensitivity to new physics, and serves as a central part in this thesis.

3

Theory

In a minimal scenario, dark matter can be realised as a vector boson arising from an extra $U(1)_X$ symmetry spontaneously broken by a scalar particle charged under the particular symmetry. Interactions with the SM can then occur through a dark portal scenario commonly referred to as the Higgs portal. Through the operator product expansion a weak effective theory is formulated and the dark portal contributions to flavour-changing decays can be expressed as contributions to the Wilson coefficients, from which branching fractions for weak decays of rare mesons can be calculated. This chapter is divided into two parts, where in the first part the theory of a Higgs portal model is described, and in the second further discussed in the aspect of flavour physics and the possibility to probe such extensions of the SM.

3.1 Vectorial dark matter model

An intuitive and simple model of vectorial dark matter is that it stems from an extra $U(1)$ gauge group, denoted $U(1)_X$ [30]. This is a natural choice, since vector bosons in the Standard model (SM) arise from broken gauge groups. Assuming the SM particles to be neutral under $U(1)_X$, they are decoupled from it. The collection of the $U(1)_X$ gauge group and all hypothetical particles that may live under it, is commonly referred to as the *dark sector*.

Vector bosons in the SM are given mass through the Higgs mechanism that spontaneously breaks the electroweak symmetry. In order for the DM gauge boson to gain mass, it is therefore reasonable that a Higgs-like particle exists in the dark sector and spontaneously breaks the $U(1)_X$ symmetry, in a similar way as the Higgs does in the SM. The existence of such a Higgs-like particle could induce interactions between the dark and SM sector. In particular, if the particle is scalar (spin-0), renormalisable interactions can occur through the Higgs-portal [31], and further interact with the SM-fermions via Yukawa couplings.

3.1.1 A hidden $U(1)_X$ symmetry

Assuming that there exists a hidden, extra $U(1)$ gauge group, denoted $U(1)_X$, accompanied by a complex scalar field S , one can write down the most general Lagrangian [30]

$$\mathcal{L}_{\text{hidden}} = -\frac{1}{4}F_{\mu\nu}F^{\mu\nu} + (D_\mu S)^\dagger(D^\mu S) - V(S) \quad (3.1)$$

where $F_{\mu\nu}$ is the field strength tensor of the gauge field V_μ ,

$$F_{\mu\nu} = \partial_\mu V_\nu - \partial_\nu V_\mu, \quad (3.2)$$

the covariant derivative D^μ is expressed as [32]

$$D_\mu = \partial_\mu - ig_X Y_X V_\mu, \quad (3.3)$$

while $V(S)$ denotes the scalar potential. Here, Y_X denotes the charge under the $U(1)_X$ symmetry and g_X is the coupling constant.

Consider now spontaneous symmetry breaking and assume that S picks up a Vacuum Expectation Value (VEV). After symmetry breaking, the complex scalar field S can be decomposed into a scalar and pseudoscalar part ϕ_S and σ_S , and a VEV v_S [33]

$$S = \frac{1}{\sqrt{2}}(\phi_S + i\sigma_S + v_S). \quad (3.4)$$

Inserting (3.3) and (3.4) into (3.1) produces a vast amount of terms, with a well-known structure from abelian Higgs models [34]. Consider instead the unitary gauge, in which σ_S has been gauged away:

$$S = \frac{1}{\sqrt{2}}(\phi_S + v_S) \quad (\text{Unitary gauge}). \quad (3.5)$$

Although the results of this thesis rely on the computer programme **SARAH**, which use (3.4) for the full derivation, it is convenient to use (3.5) for the purposes of this chapter. Inserting (3.3) and (3.5) into (3.1), the spontaneously broken hidden Lagrangian is

$$\begin{aligned} \mathcal{L}_{\text{hidden,SSB}} = & -\frac{1}{4}F_{\mu\nu}F^{\mu\nu} + \frac{1}{2}\partial_\mu\phi_S\partial^\mu\phi_S + \frac{1}{2}g_X^2Y_X^2V_\mu V^\mu\phi_S\phi_S + \\ & + v_Sg_X^2Y_X^2V_\mu V^\mu\phi_S + \frac{1}{2}g_X^2Y_X^2v_S^2V_\mu V^\mu - V(\phi_S, v_S), \end{aligned} \quad (3.6)$$

see appendix A.1 for a derivation. Here, the vector dark matter mass can be identified with $M_V = \sqrt{g_X^2v_S^2Y_X^2}$. For further treatment, it is now in order to set the $U(1)_X$ charge. In accordance with similar models [18, 30] the charge is set to $Y_X = 1/2$. Using the expression for M_V , the gauge-scalar interaction parts of the hidden sector Lagrangian in the unitary gauge after spontaneous symmetry breaking reads

$$\mathcal{L}_{g-s} = \frac{1}{8}g_X^2V_\mu V^\mu\phi_S^2 + \frac{1}{2}g_XM_VV_\mu V^\mu\phi_S. \quad (3.7)$$

Finally, the renormalisable scalar potential $V(S)$ that can be constructed from this minimal extension reads

$$V(S) = \lambda_S(S^\dagger S)(S^\dagger S) + \mu_S^2(S^\dagger S) \quad (3.8)$$

where $\mu_S^2 < 0$ for spontaneous symmetry breaking. Spontaneous symmetry breaking of this potential term is dealt with in the next section.

Although nothing prevents kinetic mixing terms between two $U(1)$ gauge groups such as between the SM $U(1)$ group and the hidden $U(1)_X$, mixing is not considered in this thesis and consequently the mixed gauge couplings are set to zero.

3.1.2 The Higgs portal

Assuming that the particles under the hidden sector are only V_μ and S , the hidden sector can only interact with the SM sector via the Higgs portal [30],

$$V(H, S) = \lambda_{HS}(H^\dagger H)(S^\dagger S). \quad (3.9)$$

The resulting combined potential from the hidden sector (3.8), portal interaction (3.9) and the ordinary Higgs potential [34] then reads

$$V(H, S) = \mu_S^2 |S|^2 + \mu_H^2 |H|^2 + \lambda_S S^4 + \lambda_H H^4 + \lambda_{HS} |S|^2 |H|^2 \quad (3.10)$$

using the shorthand $|X|^2 = X^\dagger X$. It is also required that $\mu_H^2 < 0, \mu_S^2 < 0$. Assuming that $H = (0, \frac{\phi_H}{\sqrt{2}})$ and $S = \frac{\phi_S}{\sqrt{2}}$ in the unitary gauge, and that both ϕ_H and ϕ_S have non-vanishing VEV at the potential minimum, the tadpole equations read

$$\mu_S^2 = -\lambda_S v_S^2 - \frac{1}{2} \lambda_{HS} v_H^2 \quad (3.11)$$

$$\mu_H^2 = -\lambda_H v_H^2 - \frac{1}{2} \lambda_{HS} v_S^2, \quad (3.12)$$

see appendix A.2 for a derivation. At spontaneous symmetry breaking, the neutral component of the Higgs picks up a VEV $H^0 = \frac{1}{\sqrt{2}}(\phi_H + v_H)$, and $S = \frac{1}{\sqrt{2}}(\phi_S + v_S)$ in the unitary gauge, as previously described. Inserting this together with the expressions above for μ_H^2, μ_S^2 , the mass matrix for the pure and mixed states is obtained as [31]

$$\mathcal{M}^2 = \begin{pmatrix} 2\lambda_S v_S^2 & \lambda_{HS} v_H v_S \\ \lambda_{HS} v_H v_S & 2\lambda_H v_H^2 \end{pmatrix} \quad (3.13)$$

in the (ϕ_S, ϕ_H) basis.

From (3.13), the mass of ϕ_S is $m_{\phi_S}^2 = 2\lambda_S v_S^2$, as expected when considering such Higgs-like particles. Assuming real couplings and requiring that $v_H > 0$ and $v_S > 0$, \mathcal{M}^2 is positive definite if

$$\lambda_H > \frac{\lambda_{HS}^2}{4\lambda_S}, \quad \lambda_S > 0, \quad (3.14)$$

see appendix A.3 for derivation. The mass matrix (3.13) can be diagonalised by $Z^H \mathcal{M}^2 Z^{H,\dagger}$, where

$$Z^H = \begin{pmatrix} \cos \alpha & \sin \alpha \\ -\sin \alpha & \cos \alpha \end{pmatrix} \quad (3.15)$$

and the angle α satisfies

$$\tan 2\alpha = \frac{\lambda_{HS} v_H v_S}{\lambda_S v_S^2 - \lambda_H v_H^2}. \quad (3.16)$$

Applying the diagonalisation, the mass squared eigenvalues are [35]

$$m_{H_1, H_2}^2 = \lambda_H v_H^2 + \lambda_S v_S^2 \pm \frac{\lambda_S v_S^2 - \lambda_H v_H^2}{\cos 2\alpha}. \quad (3.17)$$

where H_1 and H_2 represent the physical, observable particles. Note that when setting $\alpha = 0$, the expressions (3.17) reduces to the diagonal of (3.13) and implies

that $\lambda_{HS} = 0$. For this reason, α can be thought of as a mixing angle in the Higgs-sector. Furthermore, since the matrix Z^H diagonalises the mass matrix, new mass eigenstates can be defined as

$$\begin{pmatrix} H_1 \\ H_2 \end{pmatrix} = \begin{pmatrix} \cos \alpha & \sin \alpha \\ -\sin \alpha & \cos \alpha \end{pmatrix} \begin{pmatrix} \phi_S \\ \phi_H \end{pmatrix}, \quad (3.18)$$

leaving two eigenstates defined as mixings between ϕ_H and ϕ_S , parametrised by the mixing angle α . The mixing implies that both of these will couple to SM and DM states, thus representing a two-portal scenario.

Subsequent to symmetry breaking, the Yukawa terms of the SM Lagrangian reads

$$\mathcal{L}_{SM}^Y = -\frac{\phi_H}{v_H} \sum_f m_f \bar{f} f \quad (3.19)$$

where $f = q, \ell$. Rotating to mass eigenstates by

$$\begin{pmatrix} \phi_S \\ \phi_H \end{pmatrix} = \begin{pmatrix} \cos \alpha & -\sin \alpha \\ \sin \alpha & \cos \alpha \end{pmatrix} \begin{pmatrix} H_1 \\ H_2 \end{pmatrix}, \quad (3.20)$$

this interaction term reads

$$\mathcal{L}_{SM,rot}^Y = -\frac{H_1 \sin \alpha + H_2 \cos \alpha}{v_H} \sum_f m_f \bar{f} f. \quad (3.21)$$

These interactions are what will serve as the testable portal between the SM and dark sector in the subsequent analysis of flavour changing processes. Similarly, the interactions between gauge bosons and H_1 and H_2 are [35]

$$(H_1 \sin \alpha + H_2 \cos \alpha)(2M_W^2 W_\mu^+ W^{-\mu} + M_Z^2 Z_\mu Z^\mu)/v_H. \quad (3.22)$$

Trilinear couplings between H_1 and H_2 also arise, see reference [35] for a full list. Note however that in my notation, H_2 is identified as the SM Higgs.

Using the rotations, the hidden Lagrangian describing gauge-scalar interactions after spontaneous symmetry breaking (3.7) can also be rotated to these new mass eigenstates,

$$\begin{aligned} \mathcal{L}_{g-s} = & \frac{1}{8} g_X^2 V_\mu V^\mu (H_1 H_1 \cos^2 \alpha - 2H_1 H_2 \cos \alpha \sin \alpha + \sin^2 \alpha H_2 H_2) + \\ & + \frac{1}{2} g_X m_V V_\mu V^\mu (H_1 \cos \alpha - H_2 \sin \alpha). \end{aligned} \quad (3.23)$$

In this formulation, the free parameters are

$$\lambda_H, \quad \lambda_{HS}, \quad \lambda_S, \quad v_S, \quad g_X, \quad v_H \quad (3.24)$$

with the requirements

$$\lambda_H > \frac{\lambda_{HS}^2}{4\lambda_S}, \quad \lambda_S > 0, \quad v_S > 0 \quad (3.25)$$

and the masses for our new particles are given by (3.17) and

$$m_V^2 = g_X^2 v_S^2 / 4. \quad (3.26)$$

The free parameters can be traded for the set $(M_{H_1}, M_{H_2}, \sin \alpha, v_H, \lambda_{HS}, g_X)$ using the relations

$$\lambda_H = \frac{M_{H_2}^2}{2v_H^2} + \frac{\sin^2 \alpha (M_{H_1}^2 - M_{H_2}^2)}{2v_H^2} \quad (3.27)$$

$$\lambda_S = \frac{2\lambda_{HS}^2 v_H^2}{(M_{H_1}^2 - M_{H_2}^2) \sin^2 2\alpha} \left(\frac{M_{H_1}^2}{M_{H_1}^2 - M_{H_2}^2} - \sin^2 \alpha \right) \quad (3.28)$$

$$v_S = \frac{\sin 2\alpha}{2\lambda_{HS} v_H} (M_{H_1}^2 - M_{H_2}^2) \quad (3.29)$$

This new set $(M_{H_1}, M_{H_2}, \sin \alpha, v_H, \lambda_{HS})$ can be traded for $(M_{H_1}, M_{H_2}, \sin \alpha, v_H, g_X, M_V)$ via the relations

$$v_S = \frac{2M_V}{g_X} \quad (3.30)$$

$$\lambda_H = \frac{M_{H_2}^2}{2v_H^2} + \frac{\sin^2 \alpha (M_{H_1}^2 - M_{H_2}^2)}{2v_H^2} \quad (3.31)$$

$$\lambda_S = \frac{g_X^2}{8M_V^2} (M_{H_1}^2 (1 - \sin^2 \alpha) + M_{H_2}^2 \sin^2 \alpha) \quad (3.32)$$

$$\lambda_{HS} = \frac{\sin 2\alpha (M_{H_1}^2 - M_{H_2}^2) g_X}{4M_V v_H} \quad (3.33)$$

Using this last set of free parameters, it is sensible to require that the mass of either H_1 or H_2 corresponds to the usual SM Higgs mass. In this work, M_{H_2} is taken to be $\equiv M_{\text{Higgs}}$. Furthermore, for W and Z bosons to receive sensible masses, v_H should correspond to the usual SM Higgs VEV. With these requirements, the free parameters consist of the set $(M_{H_1}, \sin \alpha, g_X, M_V)$. See appendix A.4 for the derivation of these substitutions.

3.2 Flavour physics

At tree level, flavour changing neutral currents (FCNC) do not exist in the SM, but arise at the 1-loop level [8]. Consequently, the branching fractions of flavour changing (FC) processes are heavily suppressed, and further so due to the Glashow-Iliopoulos-Maiani suppression at loop level and the smallness of the Jarlskog commutator [36]. These quirks of the SM make it possible for effects of new physics to compete with the SM amplitudes.

Subsequent to electroweak symmetry breaking, interactions between the physical SM Higgs and fermions arise from the present Yukawa couplings. Through these interaction terms, FCNC transitions at the 1-loop level, and of course at higher level, can be constructed with the help of the flavour changing W^\pm -vertex. The Feynman

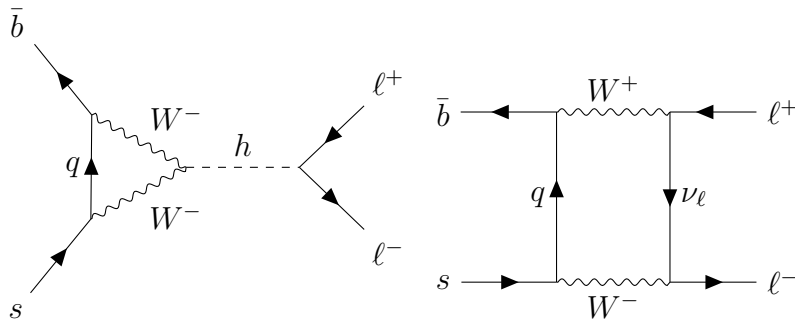


Figure 3.1: Examples of penguin (left) and box (right) diagrams for FCNC transitions related to the decay of $B_s^0 \rightarrow \ell^+ \ell^-$. Here, $q = u, c, t$.

diagrams of these interactions are commonly referred to as box and penguin diagrams. Examples of box and penguin diagrams related to the rare decay of the B_s^0 meson are shown in figure 3.1. For the hidden $U(1)$ extension previously described, the penguin diagram receives a contribution: either H_1 or H_2 can take h 's place here.

In general, the 1-loop diagrams arising in extensions of the SM are cumbersome to compute, and plenty. Moreover, they arise at an energy scale around the mass of the W -boson, $\mu \sim M_W$. This is well above the energy scale where, for example, b -physics takes place, which is at about the mass of the b -quark $\mu \sim M_b$. At this scale, electroweak interactions can be viewed as pointlike. The general strategy to evaluate a Feynman amplitude at the reference scale $\mu = \bar{\mu}$ is therefore to separate long- and short-distance effects of the theory through the Operator Product Expansion (OPE) where long-distance effects occur at scales lower than $\bar{\mu}$ and short distance effects occur at scales higher than $\bar{\mu}$ [37]. The former are generally non-perturbative effects while the latter are perturbative. These perturbative, short distance effects are encoded in the so called *Wilson coefficients* (WC) and can be calculated in perturbation theory due to the asymptotic freedom of QCD [37]. However, once the OPE has been performed and matched to the full theory, usually at the electroweak scale $\sim M_W$, the WCs carry explicit dependence on this scale. They define the theory at this particular scale while b -physics takes places at scales $M_b \ll M_W$. The second step is therefore to evolve the WCs down to the scale $\mu \sim M_b$ through the *renormalization group equations*. The WCs can then be plugged in to the general branching fraction expressions, and compared with experimental results.

A brief overview of these steps are given in the following subsections. Starting with the operator product expansion, WCs are identified and given in the basis relevant to flavour physics. The renormalization group equations are presented, and expressions for the observable branching fractions are given.

3.2.1 Operator product expansion in weak decays

While strong interactions bind hadrons together, at an energy scale $\Lambda_{QCD} \sim 0.2$ GeV, weak decays are mediated by the weak interactions of quarks, occurring at an energy scale $\Lambda_W \sim M_W \sim 80$ GeV. The energy scale where b -physics takes place is at

the scale of $M_b \sim 4.18$ GeV, much less than M_W . It is thus convenient to describe the transitions relevant to decay of B -mesons as an effective field theory, where the prescription for doing exactly this is the Operator Product Expansion (OPE). The expansion uses the fact that the momentum carried by propagators such as W^\pm are much lower than M_W , for in weak decays the momentum is of the same order as the decaying meson. As an example, if the decaying particle is a B -meson, then its momentum $k \sim M_b \ll M_W$, and thus the propagator term can be expanded in series of $\sum_{n=0}^{\infty} (k^2/M_W^2)^n$ [36]. Keeping the dominant term and discarding higher order ones, the propagator has instead been turned into a pointlike vertex. This is the main idea of OPE; electroweak operators are replaced by pointlike vertices, accompanied by effective coupling constants, the WCs. The general structure of an expanded amplitude can be written

$$\mathcal{A}_W = \langle -\mathcal{H}_{\text{eff}} \rangle + \mathcal{O}\left(\frac{k^2}{M_W^2}\right), \quad \mathcal{H}_{\text{eff}} = C(\mu)\mathcal{Q}. \quad (3.34)$$

Here, the effective Hamiltonian \mathcal{H}_{eff} contains only the leading order term in the series expansion $\sum_{n=0}^{\infty} (k^2/M_W^2)^n$. Higher order terms can safely be neglected, due to $k \ll M_W$. For the studies of weak decays of hadrons, the widely used generic effective weak Hamiltonian is [37]

$$\mathcal{H}_{\text{eff}} = \frac{G_F}{\sqrt{2}} \sum_i V_{\text{CKM}}^i C_i(\mu) \mathcal{Q}_i \quad (3.35)$$

where G_F is the Fermi coupling constant and V_{CKM}^i are the Cabbibo-Kobayashi-Maskawa (CKM) matrix elements [37]. As before, the \mathcal{Q}_i 's are operators that represent the effective vertex in question while C_i are the WCs that describe how strong the operators presence is [37]. Finally, μ is the considered energy scale of the theory. The $C_i(\mu)$ encapsulates all physics related to their respective operator at scales above μ and can be induced at tree level and higher order loop corrections. Due to the structure of the effective Hamiltonian, new physics (NP) contributions from extensions of e.g. the SM to the WCs can be included simply by

$$C_i(\mu) = C_i(\mu)_{SM} + C_i(\mu)_{NP} \quad (3.36)$$

i.e. all new physics contributions, at some arbitrary scale μ is absorbed into $C_i(\mu)_{NP}$. The next issue to deal with is therefore the actual computation of the WCs. First however, since the choice of operator basis and normalization of the WCs are arbitrary, I will briefly state the basis in which the weak effective theory is defined for this thesis.

3.2.2 The standard operator basis

While there are several choices of basis for the effective weak Hamiltonian (3.35), the machinery of `FlavBit` and `SuperIso`, two of the computer programs used in this

thesis, adopts the Standard Operator Basis [38]:

$$\mathcal{O}_1 = (\bar{s}\gamma_\mu T^a P_L c)(\bar{c}\gamma^\mu T^a P_L b), \quad (3.37)$$

$$\mathcal{O}_2 = (\bar{s}\gamma_\mu P_L c)(\bar{c}\gamma^\mu P_L b), \quad (3.38)$$

$$\mathcal{O}_3 = (\bar{s}\gamma_\mu P_L b)\left(\sum_q \bar{q}\gamma^\mu q\right), \quad (3.39)$$

$$\mathcal{O}_4 = (\bar{s}\gamma_\mu T^a P_L b)\left(\sum_q \bar{q}\gamma^\mu T^a q\right), \quad (3.40)$$

$$\mathcal{O}_5 = (\bar{s}\gamma_{\mu_1}\gamma_{\mu_2}\gamma_{\mu_3} P_L b)\sum_q (\bar{q}\gamma^{\mu_1}\gamma^{\mu_2}\gamma^{\mu_3} q), \quad (3.41)$$

$$\mathcal{O}_6 = (\bar{s}\gamma_{\mu_1}\gamma_{\mu_2}\gamma_{\mu_3} T^a P_L b)\sum_q (\bar{q}\gamma^{\mu_1}\gamma^{\mu_2}\gamma^{\mu_3} T^a q), \quad (3.42)$$

$$\mathcal{O}_7 = \frac{e}{16\pi^2} \left[\bar{s}\sigma^{\mu\nu}(m_s P_L + m_b P_R)b \right] F_{\mu\nu}, \quad (3.43)$$

$$\mathcal{O}_8 = \frac{g}{16\pi^2} \left[\bar{s}\sigma^{\mu\nu}(m_s P_L + m_b P_R)T^a b \right] G_{\mu\nu}^a, \quad (3.44)$$

$$\mathcal{O}_9 = \frac{e^2}{(4\pi)^2} (\bar{s}\gamma^\mu b_L)(\bar{\ell}\gamma_\mu \ell), \quad (3.45)$$

$$\mathcal{O}_{10} = \frac{e^2}{(4\pi)^2} (\bar{s}\gamma^\mu b_L)(\bar{\ell}\gamma_\mu \gamma_5 \ell), \quad (3.46)$$

$$Q_1 = \frac{e^2}{(4\pi)^2} (\bar{s}P_R b)(\bar{\ell}\ell), \quad (3.47)$$

$$Q_2 = \frac{e^2}{(4\pi)^2} (\bar{s}P_R b)(\bar{\ell}\gamma_5 \ell). \quad (3.48)$$

Here, the sums runs over $q = u, d, s, c, b$, m_b is the b -quark mass, m_s the s -quark mass, T^a are the $SU(3)_c$ generators and γ_μ are the Dirac matrices. $F_{\mu\nu}$ and $G_{\mu\nu}^a$ are the photon- and gluon stress tensors while g is the strong coupling, and e the elementary charge. $P_{L,R} = (1 \mp \gamma_5)/2$ are the projection operators. The above list of operators constitute the effective Hamiltonian relevant for $b \rightarrow s$ transitions [39]

$$\begin{aligned} \mathcal{H}_{\text{eff}} = & -\frac{4G_F}{\sqrt{2}} V_{tb} V_{ts}^* \left[\sum_{i=1}^{10} (C_i(\mu)\mathcal{O}_i(\mu) + C'_i(\mu)\mathcal{O}'_i(\mu)) + \right. \\ & \left. + \sum_i^2 (C_{Q_i}(\mu)Q_i(\mu) + C'_{Q_i}(\mu)Q'_i(\mu)) \right] \end{aligned} \quad (3.49)$$

where the V_{tb} and V_{ts}^* are specific CKM matrix elements. The primed operators and WCs refers to chirality-flipped versions.

For the dark portal model previously described, only Q_1 and Q_2 's respective WCs C_{Q_1} and C_{Q_2} get a contribution to their ordinary SM values. While this fact is difficult to see from what is presented, these operators are the only ones that corresponds to scalar propagators, and so models with extended Higgs sector may receive large contributions [39].

3.2.3 Computation of Wilson coefficients and renormalization group equations

In previous sections, I have briefly mentioned the WCs dependence on the energy scale μ . The time has come to explain how this dependence arises, and how the WCs are calculated for an arbitrary value of μ .

The WCs can be extracted by demanding that the amplitude in the full theory $\mathcal{A}_{\text{full}}$ is reproduced in the effective theory amplitude \mathcal{A}_{eff} . This is what is known as the *matching procedure*. In the effective theory gained by the OPE, vertices involving W -boson propagators are turned into effective vertices as discussed before. In the process of doing so, Feynman loop diagrams involving both strong and weak interactions generally become divergent. Divergences that occur both in the full and effective theory are eliminated by ordinary quark field renormalization, but new divergences can arise in the effective theory that are not present in the full theory. These additional divergences are handled through operator renormalization. Performing the renormalizations and matching the effective onto the full theory, the WCs can be extracted.

However, the resulting WCs in ordinary perturbation theory include terms proportional to $\alpha_s \ln(M_W^2/\mu^2)$, only useful when the renormalization scale $\mu \sim M_W$ since if $\mu \ll M_W$ the logarithms will become larger and have to be resummed to all orders of perturbation theory before the resulting WCs can be trusted again [37].

The solution for evolving down the WCs $C_i(\mu_W) \rightarrow C_i(\mu_b)$ in a perturbative way is to use the Renormalization Group Equations (RGE). The RGEs dictate the coupling constants dependence on the energy scale, and in the context of the effective couplings, the WCs, they are given by [36]

$$\frac{dC(\mu)}{d \ln \mu} = \gamma_Q C(\mu) \quad (3.50)$$

where γ_Q is the so called *anomalous dimension* of the operator Q [36]

$$\gamma_Q = \frac{1}{Z} \frac{dZ}{d \ln \mu} \quad (3.51)$$

and Z is the renormalization constant, dependent on the used renormalization scheme. The solution of (3.50) is [37]

$$C(\mu) = U(\mu, \mu_W) C(\mu_W) \quad (3.52)$$

where $U(\mu, \mu_W)$ is the evolution function [37]

$$U(\mu, \mu_W) = \exp \left\{ \int_{g_s(\mu_W)}^{g_s(\mu)} dg'_s \frac{\gamma_Q(g'_s)}{\beta(g'_s)} \right\} \quad (3.53)$$

where g_s is the strong $SU(3)$ coupling constant and $\beta(g'_s)$ governs the running of g_s [36]

$$\beta(g_s) = -g_s \frac{d \ln Z_{g_s}}{d \ln \mu} \quad (3.54)$$

where Z_{g_s} is the renormalization constant of the strong coupling. Hence, the WCs can be evolved down to any scale using the evolution (3.52).

Choosing the matching scale to be of order M_W and calculating the WCs to the desired order in α_s in ordinary perturbation theory, the short range interactions not only involving the W -boson but also the Z -boson and top-quark, and generally all higher mass particles are all absorbed into the WCs. What remains is the so called five quark effective theory. Evolving down the WCs to the scale $\mu_b \sim M_b$ where B -meson physics takes place, the rare meson decay branching fractions can be computed.

3.2.4 Flavour changing transitions

As discussed in section 3.2.2, the only WCs that are getting new physics contributions in this model are C_{Q_1} and C_{Q_2} . While `FlavBit` has the ability to compute likelihoods for plenty of observables, the only ones affected by $C_{Q_{1,2}}$ are the branching fractions of rare meson decays to lepton pairs. The FCNC $b \rightarrow s$ is probed by the decay $B_s^0 \rightarrow \ell^+ \ell^-$, and $b \rightarrow d$ by $B^0 \rightarrow \ell^+ \ell^-$ and the branching fraction of these decays are [39]

$$\mathcal{B}(B_q^0 \rightarrow \ell^+ \ell^-) = \frac{G_F^2 \alpha^2}{64\pi^3} f_{B_q}^2 \tau_{B_q} m_{B_q}^3 |V_{tb} V_{tq}^*|^2 \sqrt{1 - \frac{4m_\ell^2}{m_{B_q}^2}} \times \left\{ \left(1 - \frac{4m_\ell^2}{m_{B_q}^2}\right) |C_{Q_1} - C'_{Q_1}|^2 + \left| (C_{Q_2} - C'_{Q_2}) + 2 \frac{m_\ell}{m_{B_q}} (C_{10} - C'_{10}) \right|^2 \right\}, \quad (3.55)$$

where $q = d, s$. Here, α is the fine-structure constant, τ_{B_q} is the lifetime of the B -meson and f_{B_q} is its decay constant. As the main uncertainty in (3.55) comes from the decay constant [38], these decays are rather clean channels for probing FCNCs. `FlavBit` computes the branching fractions $B^0 \rightarrow \mu^+ \mu^-$, $B_s^0 \rightarrow e^+ e^-$, and $B_s^0 \rightarrow \mu^+ \mu^-$ using (3.55) as well as likelihoods based on comparisons with experimental values. For a full list of observables computable by `FlavBit`, see reference [39].

The branching fraction for $B_s^0 \rightarrow \ell^+ \ell^-$ is Charge-Parity (CP) averaged, while the experimental value is untagged. CP averages refer to the average over CP even and CP odd amplitudes [40], and the untagged approach is a way to reconstruct B -meson events experimentally [41].

The untagged branching fraction for e.g. the decay into muon pairs is related to the CP-averaged one by [38]

$$\mathcal{B}^{\text{untag}}(B_s^0 \rightarrow \mu^+ \mu^-) = \left[\frac{1 + \mathcal{A}_{\Delta\Gamma} y_s}{1 - y_s^2} \right] \mathcal{B}(B_s^0 \rightarrow \mu^+ \mu^-) \quad (3.56)$$

where

$$y_s \equiv \frac{1}{2} \tau_{B_s} \Delta\Gamma = 0.088 \pm 0.014 \quad (3.57)$$

and

$$\mathcal{A}_{\Delta\Gamma} = \frac{|P|^2 \cos(2\varphi_P) - |S|^2 \cos(2\varphi_S)}{|P|^2 + |S|^2} \quad (3.58)$$

with

$$S \equiv \sqrt{1 - 4 \frac{m_\mu^2}{M_{B_s}^2} \frac{M_{B_s}^2}{2m_\mu m_b + m_s} \frac{1}{C_{10}^{SM}} \frac{C_{Q_1} - C'_{Q_1}}{C_{10}^{SM}}} \quad (3.59)$$

$$P \equiv \frac{C_{10} - C'_{10}}{C_{10}^{SM}} + \frac{M_{B_s}^2}{2m_\mu m_b + m_s} \frac{1}{C_{10}^{SM}} \frac{C_{Q_2} - C'_{Q_2}}{C_{10}^{SM}} \quad (3.60)$$

and

$$\varphi_S = \arg S, \quad \varphi_P = \arg P. \quad (3.61)$$

Using this relation between CP averaged and untagged versions, the computed value can be compared to the experimental. A similar relation exist for the untagged decay into electron pairs.

In **FlavBit**, comparisons to experimental values are included only for the decays to muon pairs and so these are the ones that contribute to the overall likelihood. While the decay to electron pairs is not included in the likelihood, it is still computed for completeness.

4

Computational tools

The computation of Wilson coefficients for an arbitrary extension of the SM is cumbersome, to say the least. For a given model, all possible interactions must be computed, and all the Feynman diagrams contributing to the interactions. A vast amount of diagrams exist already at tree level, and at the 1-loop level where FCNCs take place, there are plenty more. Furthermore, only a small part of these may be non-vanishing. Consider you computed all these diagrams analytically in the full theory. Now you would have to do it all over again, after the OPE in order to match and extract the WCs and then run them down to the energy scale of interest, in order to evaluate the observables relevant for weak decays.

Fortunately, there exist a great amount of tools to fully automatize such procedures. In my analysis, I have implemented the complete and full theory of a Higgs-like dark portal in **SARAH** [33, 42], a program used for computing all information, including interactions and Feynman diagrams, for the model. With **SARAH**'s extension **FlavorKit** [43], analytical WCs were extracted. **SARAH** also possess the possibility to generate **SPheno** [44][45] modules for the model, that allowed for numerical computations of the WCs at a matching scale $\mu = 160$ GeV in the $\overline{\text{MS}}$ scheme. **SPheno** then exported the WCs into **wcxf** [46] files, that were read by the Python [47] package **wilson** [48] which translated the WCs into the **FlavBit** [39] basis and ran them down via RGEs to the energy scale $\mu \sim M_b$. Finally, the WCs were sent upstream into the **GAMBIT** [49] module **FlavBit** where observables were computed by **SuperIso** [38] and likelihoods were evaluated.

In this chapter I will briefly describe the different code packages and how they connect. I start with a brief overview of **GAMBIT** and its physics module **FlavBit**, culminating in the necessary steps needed to be taken in order to compute the observables. Subsequently, the various codes used in achieving the steps and their role in the implementation are presented. I conclude by describing the scans performed within the complete **GAMBIT** implementation.

4.1 GAMBIT

The Global and Modular Beyond-the-Standard-Model Inference Tool (**GAMBIT**) is, as evident by its name, a global fitting package for Beyond the Standard Model (BSM) theories. **GAMBIT** is in practice a compilation of different physics models and one scanner module, **ScannerBit** [50]. The physics modules calculates observ-

ables and likelihoods, typically with the help of external programs, referred to as backends. The scanner module samples combinations of parameters, and runs the corresponding functions in the chosen physics modules in order for each combination. The free parameters of a specified model correspond to the parameter space scanned by `ScannerBit`. All details of a scan is set in a master `YAML` file.

Adding a new model to `GAMBIT` is straightforward, and even easier is the implementation of a child model. A child model is a model that sets the values of the parents parameters via some translation function, i.e. it maps its own parameter space to the parents. This means that fundamental parameters more specified by one model are computed and sent 'upstream' to the more general parent model.

In the `GAMBIT` physics module `FlavBit`, a flavour EFT model `WC` is already implemented that takes numerical deviations from the SM `WCs` as input and performs likelihood calculation routines for the different observables. My implementation was therefore to create a child model to the parent model `WC` that takes fundamental parameters in the theory as input, calculates the contributions to the `WCs`, and sends them upstream to the parent.

4.1.1 FlavBit

The module `FlavBit` is the part ("bit") of `GAMBIT` that performs flavour physics calculations. In `FlavBit`, observables are implemented for the Minimal Supersymmetric Standard Model (MSSM) and for a flavour EFT model, named `WC` in the `FlavBit` namespace. In the former case, the user can input a SUSY Les Houches Accord (SLHA) file to perform calculations and in the latter, numerical deviations from SM `WCs` are specified directly as model parameters. Observables in the flavour EFT model are calculated via the backend code `SuperIso`.

Since the model in question for this thesis does not realize supersymmetry, but rather that the dark sector is hidden as an extension to the SM, a flavour EFT model was chosen. The `FlavBit` flavour EFT model `WC` first notifies `SuperIso` that it should perform its calculations for the SM and then passes the deviations arising from extensions of the SM, modifying the `WCs` before observables are calculated. The `WCs` possible to modify are the real and imaginary parts of $C_7^{\text{eff}}, C_9^{\text{eff}}, C_{10}, C_{Q_1}, C_{Q_2}$ where

$$C_7^{\text{eff}} = C_7 - \frac{1}{3}C_3 - \frac{4}{9}C_4 - \frac{20}{3}C_5 - \frac{80}{9}C_6 \quad (4.1)$$

$$C_9^{\text{eff}} = C_9 + Y(q^2), \quad (4.2)$$

and Y contains the short distance contributions from the four-quark operators [39]. For my model, only C_{Q_1} and C_{Q_2} were modified while the other modifications were set to zero.

`SuperIso` computes the `WCs` for the SM down to the level of next-to-next-to leading order contributions at the matching scale μ_W and then evolves them down to the

relevant scale μ_b before adding the modifications by the `FlavBit` model WC. After these modifications are added, `FlavBit` continues by using `SuperIso` to compute the branching ratios and then pass these observables back to `FlavBit` for computing the likelihood, comparing to experimental results.

Since the modifiable WCs only affect the branching ratios (see table 2 in reference [39])

$$B^0 \rightarrow \mu^+ \mu^-, \quad B_s^0 \rightarrow \mu^+ \mu^-, \quad B_s^0 \rightarrow e^+ e^- \quad (4.3)$$

$$B \rightarrow X_s \gamma, \quad B \rightarrow X_s \tau^+ \tau^-, \quad B \rightarrow X_s \mu^+ \mu^- \quad (4.4)$$

the primary likelihoods to calculate in the `GAMBIT` scan were the ones involving those. However, since the dark portal under consideration only receives contributions to C_{Q_1} and C_{Q_2} , parameters that only impact the top row of branching fractions, i.e. the purely leptonic decays and hence only these were computed.

So far, this is an appropriate workflow for the aims of this thesis. However, I want to set constraints on the fundamental parameters of the theory, not the numerical WCs. As previously discussed, the solution to this was to implement a child model that takes the fundamental parameters as input, calculates the numerical deviations to the SM WCs, and sends them upstream via a translation function.

Computing WCs from a generic Lagrangian is a tedious task. The procedure is fortunately automated and implemented in many available codes, such as `SARAH` and its inclusion of `FlavorKit`. Furthermore, `SARAH` includes the automated generation of `SPheno` code, which after compilation is able to compute the numerical BSM contributions to WCs with the input of fundamental parameters. However, `FlavorKit` and `FlavBit` work in different operator bases and so a translation between bases is required. Additionally, `SPheno` outputs the numerical WCs at matching energy scale $\mu = 160$ GeV, and so has to be evolved down before it can be included in the computations by `SuperIso`. The solution to both of these issues is handled by `wilson`, a `Python` package used for translating between operator bases and for running the WCs down to the low-energy scale, e.g. the scale $\mu \sim M_b$. The steps to be taken when writing the translation function is thus

- Implement the theory in `SARAH` and generate the `SPheno` code. This step only needs to be done once.
- Read the input parameters from `ScannerBit` and input them to `SPheno`.
- Execute `SPheno` for the current point in the parameter space.
- Translate the WCs to a base recognised by `FlavBit` using `wilson`.
- Run the WCs down to the energy scale $\mu \sim \mu_b$ using `wilson`.
- Pass the numerical deviations from the SM Wilson coefficients to the parent model.

In the following sections, the realisation of the BSM contributions to numerical WCs from the initial Lagrangian is described in terms of the codes described above, i.e. **SARAH**, **FlavorKit**, **SPheno**, and **wilson**. The full translation function that was implemented in **GAMBIT** is given in appendix C.3.2 while the child model definition for **GAMBIT** is given in appendix C.3.1.

4.2 SARAH/FlavorKit

The **Mathematica** [51] package **SARAH 3.2** [33] was initially a tool used for supersymmetric (SUSY) models, but has since version 4 [42] been extended to also being able to handle extensions of non-SUSY models such as extensions to the SM. From a model file where the user defines the gauge structure, particle content, superpotential, broken symmetries and particle mixings, **SARAH** derives the full Lagrangian and extracts all interactions after electroweak symmetry breaking. In the process of doing this, all fields in gauge eigenstates are rotated to new mass eigenstates, accompanied by calculations of the mass matrices and the diagonalization of these. Finally, tadpole equations are derived in order to find the minimum of the superpotential.

Since version 4.2, **SARAH** includes **FlavorKit**, a package able to analytically extract Wilson coefficients and/or calculate the numerical counterpart via the **SPheno** output. Additionally, the inclusion of **FlavorKit** gives the user freedom to implement new operators not initially included in **SARAH**. However, the already implemented operators are sufficient for the model in question and so only the basic functionality of **FlavorKit** is required.

A broad range of models are already implemented in **SARAH**, hence making it significantly easier to copy needed elements from other models and/or build upon existing ones. Since the model in question is an extension to the SM, the SM model file already implemented in **SARAH** was used as a basis. Another model already implemented in **SARAH** is the **U1Extensions-hiddenU1** [32], containing a significant amount of elements needed for the model of this thesis. This way of creating new models is preferred since it greatly reduces potential errors originating from typos or misdefinitions.

The **SARAH** model needs four files to build a model. First, a main model file that defines gauge groups, particle content, superpotential, symmetry breaking and field rotations. Second, a particle file, defining all particles in the model. Third, a parameters file, defining all other parameters in the model. Finally, a **SPheno** file, which controls the **Fortran** modules generation. For loading the model in **SARAH**, simply add the four separate files given in appendix C.1.1-C.1.4 to the model directory of **SARAH** and execute

```
Get [ " path/to/sarah/" ]
Start [ "VDM" ]
ModelOutput [EWSB]
```

```
MakeTeX []
```

The last line above produces a compilable L^AT_EX-file containing all output from SARAH. In the next sections, I will go through the implementation of the theory in each of these files, with the SM and U1Extensions-hiddenU1 models as a basis.

4.2.1 VDM.m

Starting with the main model file, the first step was to define the $U(1)_X$ extension to the already defined gauge fields in the SM, $SU(3) \times SU(2) \times U(1)$. This was defined by the line

```
Gauge [[4]] = { Bp, U[1], chargeX, gX, False };
```

where the last entry **False** defines whether the sums over charge indices should be expanded or not. This entry has no effect for Abelian groups. The fourth entry names the coupling constant of the gauge group.

Since the extension is detached from the SM, all SM particles are neutral under this group i.e. all the corresponding charges are set to zero. For example, the Higgs doublet was defined as

```
ScalarFields [[1]] = {H, 1, {H0, Hm}, -1/2, 2, 1, 0};
```

where the last zero is the charge under $U(1)_X$.

The definition of the scalar mediator field S was done by the line

```
ScalarFields [[2]] = {s1, 1, S1, 0, 1, 1, 1/2};
```

where the field is named s_1 , purely for making the model easier to extend to containing multiple new scalars. The second entry denotes the number of generations, S_1 is the component of the field (compare with Higgs doublet), it has neutral hypercharge, transforms as a singlet under $SU(2)$ and $SU(3)$, and has charge $1/2$ under the new gauge group $U(1)_X$.

All kinetic terms are automatically added based on this content. This means that there was no need to define the first two terms in (3.1). The scalar potential (3.10) must be added, however. The addition was rather straightforward, done by modifying the LagNoHC entry in the SM model file by

```
LagNoHC = - muH2 conj[H].H - muS12 conj[s1].s1
           - lamH conj[H].H.conj[H].H
           - lamHS1 conj[H].H.conj[s1].s1
           - lamS1 conj[s1].s1.conj[s1].s1;
```

Note that the potential is defined in SARAH with a global minus sign [52].

The rotation in the gauge sector was performed by the lines

```
DEFINITION [EWSB] [ GaugeSector ] =
{
  { {VB,VWB[3] , VBp} , {VP, VZp, VZ} , ZZ } ,
  { {VWB[1] , VWB[2] } , {VWm, conj [VWm] } , ZW }
};
```

Here, **VB** denotes the B-boson i.e. the SM $U(1)_Y$ gauge boson, **VWB** are W -bosons and **VBp** is the new $U(1)_X$ gauge boson. The **ZZ** is the mixing matrix that rotates the gauge eigenstates to the mass eigenstates **VP** (photon), **VZ** (Z -boson) and **VZP** (Z' -boson). This inclusion ensures that **SARAH** identifies the massive dark matter gauge boson Z' with the spontaneously broken symmetry $U(1)_X$. Note that the order of $\{\mathbf{VP}, \mathbf{VZP}, \mathbf{VZ}\}$ matters, they should be listed such that the first entry is the lightest particle. In this particular way of ordering, I have assumed Z' to be lighter than the Z . The second line defines a similar rotation for the charged gauge-bosons and since no new particles of this type arise in the model, this was left untouched.

The definition of symmetry breaking and the VEVs was done by the segment

```
{S1 , {vS , 1/Sqrt [2] } , {sigmaS , \[ImaginaryI]/Sqrt [2] } ,
{phiS , 1/Sqrt [2] } }
```

where the three different parts refers to the parts the field S_1 is expanded into. The first part is simply the VEV $v_S/\sqrt{2}$, the second part the pseudoscalar, and the third part the real scalar.

Rotations in the matter sector were then defined. Since there are now two scalar/pseudoscalar fields in the Higgs sector, the usual Higgs sector in the SM must be extended

```
DEFINITION [EWSB] [ MatterSector ] =
{
  { {phiS , phiH } , {hh , ZH} } ,
  { {sigmaS , sigmaH } , {Ah , ZA} } ,
  ...
}
```

where the dots refer to the SM fermions whose rotations were left untouched in this model. In the first line, the two real scalar parts of the mediator and Higgs are rotated by the Z^H matrix, that diagonalises the mass matrix, to the new mass eigenstates H_1 and H_2 i.e. the rotation described in (3.20). A similar rotation is done for the pseudoscalar parts. Again, the order matters and for this particular ordering I consider the mediator to be lighter than the ordinary Higgs.

4.2.2 particles.m

The particles file only serves to define the particle content of the theory. The definition of the new particle S was done by the following entry;

```
{S1 , { PDG -> 0 ,
```

```

Width -> 0,
Mass -> Automatic,
FeynArtsNr -> 98,
LaTeX -> "S_{1}",
OutputName -> "S1" }},

```

The **PDG** number is needed if the written model files should be readable by event generators or if the mass is given by a SLHA file. When the mass is set to automatic, it is derived from the tree level expression of the Lagrangian [33] i.e. $m_S^2 = 2\lambda_S v_S^2$, and the **PDG** number was not needed and thus set to zero. The width of the particle is unknown, and so was left undefined by setting it to zero. The **FeynArtsNr** is the number of the particle if output to a **FeynArts** model file is generated. The **LaTeX** name is simply the output name for the \LaTeX -file, and **OutputName** is needed to make sure that programs outside **SARAH** can read the name correctly.

Subsequent to electroweak symmetry breaking, there are two generations of physical particles as described before, H_1 and H_2 . When only the Higgs is present, there is just one particle in the Higgs-sector. Therefore, the mass eigenstates **hh** needed to be extended by one entry,

```

{hh    , { Description -> "Higgs" ,
          PDG -> {35,25} ,
          ...

```

where the dots are entries left untouched. The **PDG** numbers in this case are set in order to be identified correctly. **PDG 25** corresponds to the SM Higgs, while **35** corresponds to additional Higgs-like bosons [53]. Since H_1 was identified with the physical mediator particle, it receives **PDG** number 35. The same was done for the rotated pseudoscalar sector, **Ah**. Furthermore, the pseudoscalars are generally gauged away, getting eaten by the massive vector bosons. This was done by defining

```

{VZ,    { Description -> "Z-Boson" ,
          Goldstone -> Ah[{1}] }},
{VZp,   { Description -> "Z'-Boson" ,
          Goldstone -> Ah[{2]}}},
{gZp,   { Description -> "Z'-Ghost" }},

```

Here, the ghost particle associated with the new Z' -boson was defined as well. Recall that the Z' -boson is the vector boson arising from the broken $U(1)_X$ symmetry in **SARAH**. Note that a convenient way of defining the bosons was used here: **SARAH** uses a global parameters and particles file, containing often used particles or parameters. The user then only needs to supply the description of the object, and **SARAH** will collect all information from the global files. The user can also modify certain blocks in the global files. By adding the entry **Goldstone** this particular block was modified in this model, but the rest of the information contained in the global parameters file was used.

4.2.3 parameters.m

The parameters file defines the free parameters in the model. They can have dependences on other parameters, numerical, or **SPheno** dependences. The new gauge couplings was defined by

```
{g1X,      { Description -> "Mixed_Gauge_Coupling_2" ,
            LesHouches -> {gauge, 10} ,
            LaTeX -> "g_{YX}" ,
            OutputName -> gYX }},

{gX1,      { Description -> "Mixed_Gauge_Coupling_1" ,
            LesHouches -> {gauge, 11} ,
            LaTeX -> "g_{XY}" ,
            OutputName -> gXY }},

{gX,       { Description -> "chargeX-Coupling" ,
            LaTeX -> "g_{X}" ,
            Dependence -> None,
            LesHouches -> {gauge, 4} ,
            OutputName -> gX }},
```

In addition to the new, pure g_X coupling also mixed gauge couplings were introduced, that control the strength of gauge kinetic mixing. These are set to zero in further computations since I do not consider kinetic mixing, but it is rather straightforward to turn on mixing by setting them to non-zero values. The entry **LesHouches** simply defines what block in an output SLHA file the value is given, and the number it has.

In a similar manner, the rest of the free parameters were defined as

```
{vS,      { LaTeX -> "v_{S}" ,
            Dependence -> None,
            OutputName -> vS,
            Real -> True,
            LesHouches -> {VDM,1} }},

{lamH,    {OutputName -> lamH,
            LaTeX -> "\\lambda_H" ,
            LesHouches -> {VDM,2} }},

{lamHS1,  {OutputName -> lamHS1,
            LaTeX -> "\\lambda_{HS1}" ,
            LesHouches -> {VDM,3} }},

{lamS1,   {OutputName -> lamS1,
            LaTeX -> "\\lambda_{S1}" ,
            LesHouches -> {VDM,4} }},

{muH2,    {OutputName -> muH2,
```

```

LaTeX -> "\\mu_{H}^2",
LesHouches -> {VDM,5}},
{muS12, {OutputName -> muS12,
LaTeX -> "\\mu_{S1}^2",
LesHouches -> {VDM,6}}},

```

Although μ_S^2 and μ_H^2 is solved via the tadpole equations, writing them to SLHA is still convenient, and all parameters appearing in `VDM.m` must be defined.

The final addition will be the scalar mixing matrix, Z^H . It was defined as

```

{ZH, { Description -> "Scalar-Mixing-Matrix",
DependenceOptional -> None,
DependenceNum -> None,
Dependence -> {{Cos[Alpha], Sin[Alpha]},
{-Sin[Alpha], Cos[Alpha]}}},
}},

```

Here, `Dependence` defines a dependence used in analytical calculations where Z^H as defined in (3.15) was used.

The angle α used above needs to be defined as well

```

{Alpha, { Description -> "Scalar mixing angle",
Dependence -> None,
DependenceOptional -> None,
DependenceNum -> None,
DependenceSPheno -> ArcTan[lamHS1 vS vH
/ (lamS1 vS^2 - lamH vH^2)]/2 }},

```

Here, a `SPheno` dependence was set. This was done in order to ensure that `SPheno` really uses the correct parametrisation when running calculations of the numerical WCs. Again, the information about α was collected from the global parameters file, but the `SPheno` dependence was overwritten.

4.2.4 SPheno.m

The last input file `SARAH` needs is the information for building the `SPheno` modules. It starts with the line

```
OnlyLowEnergySPheno = True
```

and is present because `SPheno` is generally meant for SUSY models and extensions to such models. Setting the above particular setting to true, `SPheno` performs no RGE running but only performs matching at the electroweak scale [52] and can then be used also for non-SUSY models. The resulting WCs therefore needs to be run down to the scale where b -physics takes place, i.e. the scale of the b -quark mass $\mu_b \sim m_b$, a discussion postponed for now.

4. Computational tools

Working with a low energy version of **SPheno**, the input parameters need to be specified first, i.e. the fundamental parameters considered in this model. This block reads

```
MINPAR={ {1,LambdaHINPUT},
          {2,LambdaHS1INPUT},
          {3,LambdaS1INPUT},
          {4, gXINPUT},
          {5, vSINPUT},
          {6, vHINPUT}}
```

Next, **SPheno** was told to solve tadpole equations for μ_H^2 and μ_S^2 by

```
ParametersToSolveTadpoles = {muS12,muH2};
```

The block concerning matching conditions was performed for the SM. No matching conditions for the extension exist, and so this block was left untouched. The next block reads

```
BoundaryLowScaleInput={
  {gX,gXINPUT},
  {g1X,0},
  {gX1,0},
  {lamH, LambdaHINPUT},
  {lamHS1, LambdaHS1INPUT},
  {lamS1, LambdaS1INPUT},
  {vS,vSINPUT},
  {vH,vHINPUT}
};
```

This simply means that for the low scale input, **SPheno** was told to use the parameters defined in the **MINPAR** block, but since no kinetic mixing was considered the mixed gauge couplings g_{1X} and g_{X1} are set to zero. Equivalently, g_{X1} or g_{1X} can be defined in the **MINPAR** block instead and set to zero later.

The rest of this file reads the same as for the SM. Default input values for the parameters in question can be set as

```
DefaultInputValues = {LambdaHINPUT -> 0.2,
                      LambdaHS1INPUT -> 0.2
                      LambdaS1INPUT -> 0.1
                      gXINPUT -> 0.7,
                      vSINPUT -> 200,
                      vHINPUT -> 246.22
                      };
```

which was then automatically printed as input values to the executable **SPheno** code.

4.3 SPheno

By executing the command

```
MakeSPheno []
```

in **SARAH** subsequent to loading a model, **Fortran** modules used for compiling the **SPheno** model are generated automatically. The input SLHA file is also generated based on the default parameters specified in the **SPheno.m** file.

SPheno outputs numerical WCs in the **FlavorKit** basis to a **wcxf** file if flag 79 in the input SLHA file is set to 1. Moreover, these files can effortlessly be passed to other codes since the file format is widely supported. This feature was the main motivation as to why using **SPheno** instead of implementing the analytical WCs outputted from **SARAH**.

The **wcxf** output is separated into two files: one for the quark-flavor violating sector, and one for the lepton-flavor violating sector. As **FlavBit** only deals with $b \rightarrow s$ and $b \rightarrow d$ transitions, i.e. quark-flavour violating transitions, only the first sector was used. These were outputted at the renormalization scale $\mu = 160$ GeV.

However, the **wcxf** files are given the same automatic default names every time the **SPheno** model has run. This is undesirable when running multiple processes at the same time, as the outputs could overwrite each other. It was therefore preferred to have **SPheno** output the files with names specified by the user, via e.g. the command line instead. This was done by adding

```
Call get_command_argument(3,wcxfFileName)
If (len_trim(wcxfFileName)==0) Then
  wcxfFileName="WC.VDMv2_1.json"
Else
  wcxfFileName=trim(wcxfFileName)
End if
```

to line 160 in **SPhenoVDM.f90**, and line 6133 in **InputOutput_VDM.f90** was replaced with

```
Open(123, file=wcxfFileName, status="unknown")
```

Finally, the file name string had to be defined, which was done by replacing line 35 in **InputOutput_VDM.f90** with

```
Character(len=120)::inputFileName, outputFileName, wcxfFileName
```

Once these additions and replacements were done in the automatically generated **Fortran** modules by **SARAH**, the model was compiled in **SPheno**. For compiling, download and install **SPheno**, enter the root directory of the installation, create a new subdirectory, copy the **SARAH** output to this directory and compile it via the commands [43]

```
> cd [$SPheno]
> mkdir VDM
> cp [$SARAH]/Output/VDM/EWSB/SPheno/* VDM/
> make Model=VDM
```

This will create a runnable program `SPhenoVDM` in `[$SPheno]/bin` that accepts command line arguments for input SLHA name, output name, and `wcxf` output name.

4.4 wilson

The Python package `wilson` is built for the purpose of translating `wcxf` files from different bases, matching and running numerical WCs down to the desired scale. Although translation to `FlavBit` is absent, `FlavBit` shares basis with `EOS`, available in `wilson`. Hence, the WCs were translated to `EOS` basis, and then evolved down to the μ_b scale. This was in principle done via the command

```
match_run(scale=4.18, eft="WET", basis="EOS")
```

Since the output WCs from `SPheno` were already matched to the weak effective theory (WET), no matching was performed by `wilson`, only necessary basis translations and the running of the renormalisation group equations were performed. Note that both `SPheno` and `wilson` operates in the $\overline{\text{MS}}$ renormalization scheme. However, an important remark is that `FlavBit` and `EOS` has a small difference in their bases,

$$C_{Q_1}^{\text{FlavBit}} = \frac{m_b}{m_e} C_S^{\text{EOS}}, \quad C_{Q_2}^{\text{FlavBit}} = \frac{m_b}{m_e} C_P^{\text{EOS}} \quad (4.5)$$

where the m_e comes from the fact that three different C_S were obtained in the `EOS` basis: `b->see::cS`, `b->smumu::cS`, and `b->stautau::cS`. Taking the C_S for any other lepton pair and dividing this by the specific lepton mass, the same is obtained i.e.

$$C_{Q_1}^{\text{FlavBit}} = \frac{m_b}{m_e} C_S^{b \rightarrow see} = \frac{m_b}{m_\mu} C_S^{b \rightarrow smumu} = \frac{m_b}{m_\tau} C_S^{b \rightarrow stautau} \quad (4.6)$$

Same reasoning follows for C_P . Hence, it was sufficient to only extract the `b->see::cS` and `b->see::cP` coefficient and use the first relation as the final step to get the WCs in the `FlavBit` basis. For the complete `EOS` basis, see reference [54].

4.5 Performed GAMBIT runs

Five different scans were performed for the model in question using different samplers that are part of `ScannerBit`. Two scans were performed sampling both M_{H_1} and $\sin \alpha$, producing 2D surface plots of the likelihood. Three scans were performed over M_{H_1} , holding $\sin \alpha$ fixed to different values, producing plots of the branching fractions variation with M_{H_1} . In all these scans, $M_{H_2} = 125.09$ GeV and $v_H = 246.22$ GeV i.e. fixed to their SM values. Initial tests showed that variation of M_V and g_X had little to no impact on the WCs and were therefore set to the same constant values for all scans. Initial tests also showed that the branching fractions converged

Scan	Sampler	Number of points	M_{H_1} [GeV]	$\sin \alpha$	M_V [GeV]	g_X
1	<code>Diver</code>	$N_P = 2 \times 10^4$	$[10^{-2}, 70]$	$[10^{-3}, 1]$	30	0.1
2	<code>MultiNest</code>	$N_{\text{live}} = 2 \times 10^4$	$[10^{-2}, 70]$	$[10^{-3}, 1]$	30	0.1
3	<code>SquareGrid</code>	$N = 3 \times 10^5$	$[10^{-2}, 30]$	10^{-3}	30	0.1
4	<code>SquareGrid</code>	$N = 3 \times 10^5$	$[10^{-2}, 30]$	10^{-2}	30	0.1
5	<code>SquareGrid</code>	$N = 3 \times 10^5$	$[10^{-2}, 30]$	10^{-1}	30	0.1

Table 4.1: Values for the different scans. In the different samplers, points refer to population density (N_P), live points (N_{live}) and evenly spaced grids (N). See text for explanation. For all runs, the branching fractions of the decays $B_0^s \rightarrow \mu^+\mu^-$, $B^0 \rightarrow \mu^+\mu^-$ and $B_s^0 \rightarrow e^+e^-$ were computed.

to a certain value for large M_{H_1} and so the ranges were set appropriately.

Both samplers `Diver` and `MultiNest` included in `ScannerBit` are suitable for the 2D scans, but operates on different sampling algorithms. `Diver` is a differential evolution sampler that evolves a population of points (N_P) in parameter space. Generations of these are chosen by a form of vector addition between members of the population, making the sampler similar to a random walk with a step size provided by the population [50]. In contrast, `MultiNest` operates on the principles of nested sampling, which instead samples the posterior in nested shells of probability. The set of live points (N_{live}) is continually updated by replacing the lowest-likelihood point in each iteration with a better point [50]. The live points split into clusters that shrink around the peaks of the posterior as the algorithm progresses. Due to both samplers being suitable, but with very different algorithms, two identical scans were performed using each of the samplers. The `Diver` convergence threshold was set to 10^{-4} and `MultiNest` tolerance level to 10^{-3} .

For the one-dimensional scans a simple `SquareGrid` sampler was chosen, which simply samples distinguished points with spacing dependent on the parameter prior. For all parameters scanned over, a logarithmic prior was chosen since the parameters span a few magnitudes. The logarithmic prior was also used in the 2D scans.

A full list of runs, choice of samplers, and values of the fundamental parameters is presented in table 4.1. The details of each run was set through a master `YAML` file, specified by the user. For an example of a `YAML` file used, see appendix C.3.3. All scans were run on Chalmers Centre for Computational Science and Engineering (C3SE) computer cluster Vera, while initial tests were performed on National Supercomputer Centre (NSC) cluster Tetralith, both part of the Swedish National Infrastructure for Computing (SNIC). For instructions on how to build `GAMBIT` on Vera and Tetralith, see appendix B.1 and B.2, respectively.

5

Results

The aim of this chapter is to produce constraints on the fundamental parameters of a dark portal model extension of the SM. I will address this goal by comparing the branching fractions for B^0 and B_s^0 decays into muon pairs as predicted by the dark portal model with the corresponding experimental measurements.

Results of this work are summarised in two types of graphs: Branching fractions and likelihood surface plots. The former was obtained using three **GAMBIT** scans in which the sine of the mixing angle has been fixed to the values $\sin \alpha = 10^{-3}, 10^{-2}, 10^{-1}$ while the mass of the additional Higgs boson M_{H_1} has been varied within the range $[10^{-2}, 30]$ GeV. The latter was obtained using two **GAMBIT** scans, where both $\sin \alpha$ and M_{H_1} have been varied over the ranges $[10^{-3}, 1]$ and $[10^{-2}, 70]$ GeV, respectively, using two different sampling methods: **Diver** and **MultiNest**. For all scans, the dark matter mass M_V and the additional $U(1)_X$ gauge coupling constant g_X have been fixed to $M_V = 30$ GeV and $g_X = 0.1$ since varying those has minimal to no impact on the computed observables. The details of all scans can be found in section 4.5.

5.1 Branching fractions

The computed branching fractions $\mathcal{B}(B_s^0 \rightarrow \mu^+ \mu^-)$ and $\mathcal{B}(B^0 \rightarrow \mu^+ \mu^-)$ are depicted along with experimental measurements and SM predictions in figures 5.1 and 5.2. The branching fraction $\mathcal{B}(B_s^0 \rightarrow e^+ e^-)$ is depicted with SM prediction in figure 5.3.

The branching fractions are found to have the same trend when considering the dark portal model for different values of $\sin \alpha$. In fact, they tend to offset along the M_{H_1} axis by a factor ten, when $\sin \alpha$ is increased by a factor ten, implying a linear relation between them. For example, the minima in figures 5.1 and 5.2 occur at roughly $M_{H_1} = 0.04, 0.4, 4$ for $\sin \alpha = 0.001, 0.01, 0.1$. The overall shape is unchanged. For large M_{H_1} , the branching fractions converges at the same value, independent from the choice of $\sin \alpha$. Note also that the experimental value reported in these figures has statistical and systematic errors $\pm 0.6_{-0.2}^{+0.3} \times 10^{-9}$ for $\mathcal{B}(B_s^0 \rightarrow \mu^+ \mu^-)$ and $\pm 1.5 \times 10^{-10}$ for $\mathcal{B}(B^0 \rightarrow \mu^+ \mu^-)$, implying that both the SM and dark portal prediction except in a small region around the minima lies within the uncertainty of the experimental results in figure 5.1 while only some values of the dark portal prediction lie within the uncertainty in figure 5.2. See table 2.1 for a full overview of experimental measurements.

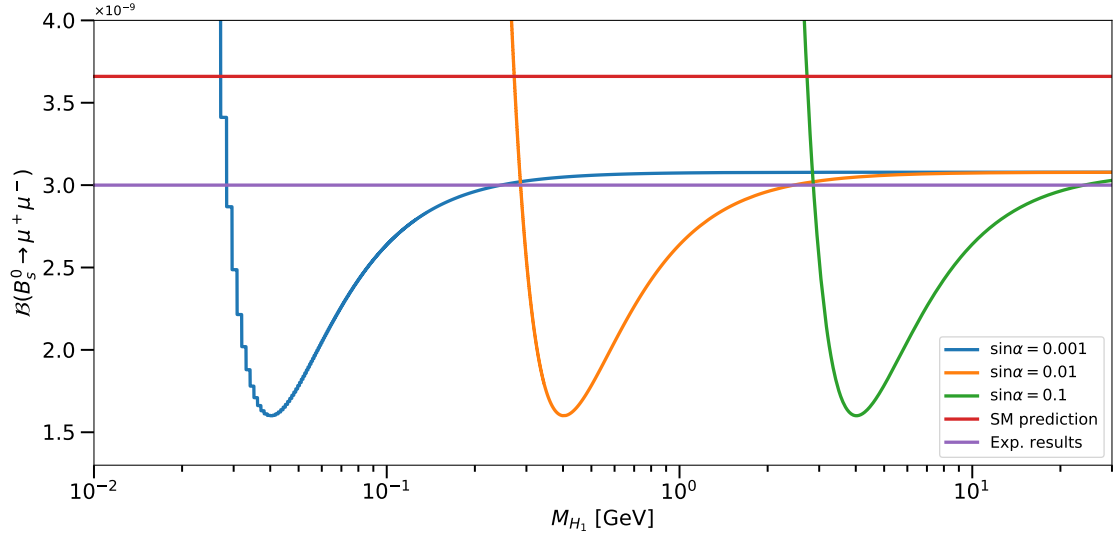


Figure 5.1: Branching fraction of the decay $B_s^0 \rightarrow \mu^+ \mu^-$ as a function of the additional Higgs-like boson mass M_{H_1} in the dark portal model, for three distinct values of the sine of the mixing angle $\sin \alpha = 0.001, 0.01, 0.1$ (blue, orange, green). The Standard Model prediction (red) and experimental measurements (magenta) are presented for comparison. Uncertainties for the experimental value are given in table 2.1.

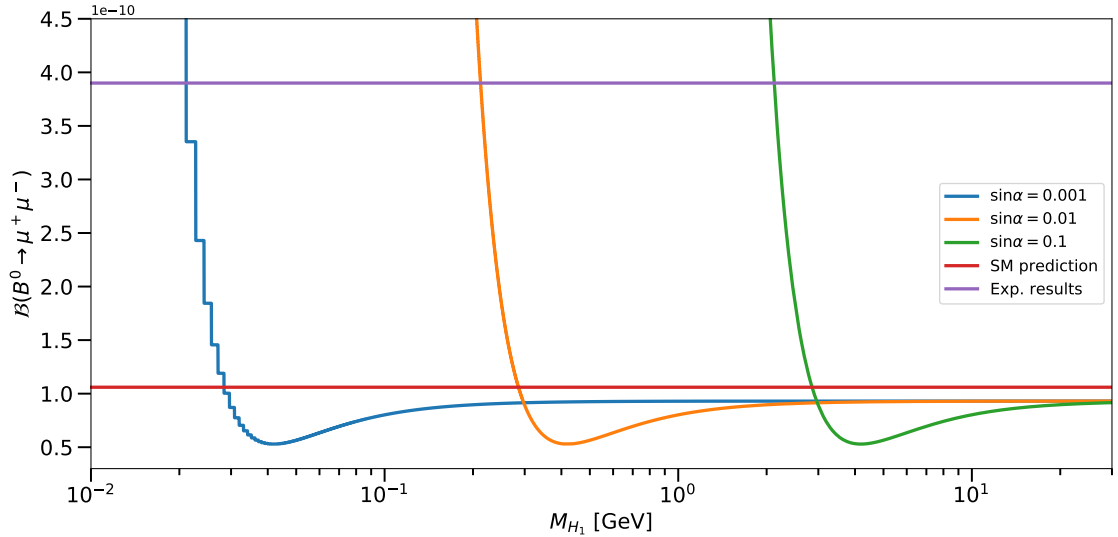


Figure 5.2: Branching fraction of the decay $B^0 \rightarrow \mu^+ \mu^-$ as a function of the additional Higgs-like boson mass M_{H_1} in the dark portal model, for three distinct values of the sine of the mixing angle $\sin \alpha = 0.001, 0.01, 0.1$ (blue, orange, green). The Standard Model prediction (red) and experimental measurements (magenta) are presented for comparison. Uncertainties for the experimental value are given in table 2.1.

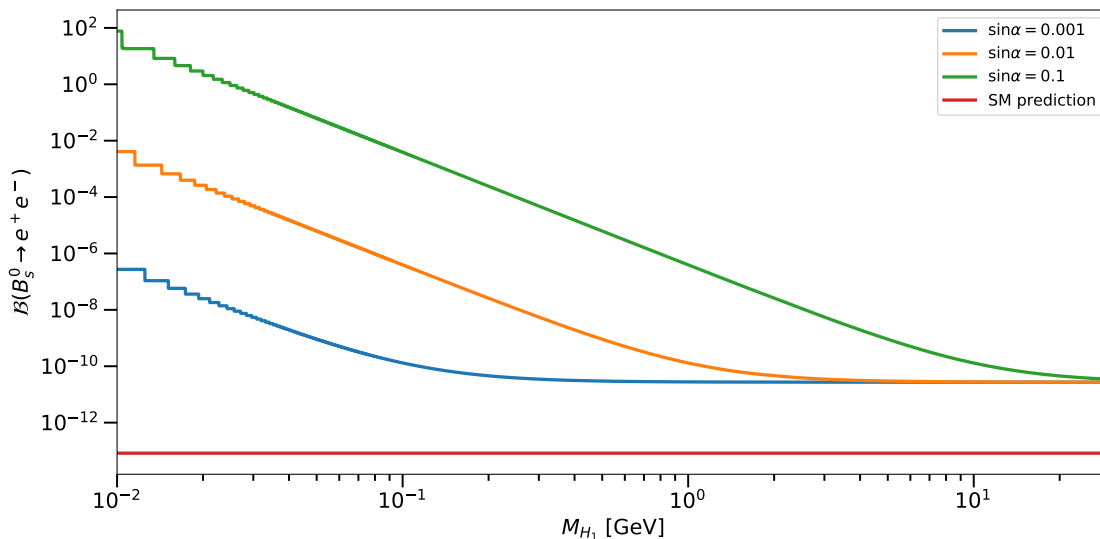


Figure 5.3: Branching fraction of the decay $B_s^0 \rightarrow e^+e^-$ as a function of the additional Higgs-like boson mass M_{H_1} in the dark portal model, for three distinct values of the sine of the mixing angle $\sin \alpha = 0.001, 0.01, 0.1$ (blue, orange, green). The Standard Model prediction (red) is presented for comparison.

It is clear that light H_1 gives rise to large branching fractions. As M_{H_1} increases, the branching fractions quickly decrease until they reach a minimum, from where they increase again and converge towards a fixed value slightly less than what is predicted from the SM. In order to explain this, consider the second absolute value term of the second line in (3.55):

$$\left| (C_{Q_2} - C'_{Q_2}) + 2 \frac{m_\ell}{m_{B_q}} (C_{10} - C'_{10}) \right|^2. \quad (5.1)$$

As stated before, only C_{Q_1} and C_{Q_2} receives contributions when considering the dark portal extension and are positive in my computations. The Wilson coefficient C_{10} remains unchanged from its SM value, and is negative in my computations, while C_{Q_1} and C_{Q_2} are negligible in the SM.

Hence, before the minima $C_{Q_2} > C_{10}$ and after, $C_{Q_2} < C_{10}$ implying that at the minima, $C_{Q_2} \approx C_{10}$ and so they cancel giving minimal contribution to the overall branching fractions. As C_{Q_2} continues to be suppressed by the mediator mass M_{H_1} , C_{10} starts to dominate, hence the increase subsequent to the minima. At large M_{H_1} , C_{Q_2} has converged to some fixed, positive value giving a slight modification to (5.1). The overall appearance of figures 5.1 and 5.2 suggests that C_{Q_1} follows a similar evolution to C_{Q_2} , decreasing rapidly for large M_{H_1} .

The above reasoning concerning the minima is further supported when considering the decays to electron pairs, see figure 5.3. For these decays, the branching fractions are as before enhanced for small M_{H_1} and converge at the same, fixed value for large

M_{H_1} however without any visible minima. This consequence is directly connected to the term (5.1), where $\Delta C_{10} \equiv C_{10} - C'_{10}$ is controlled by the factor $2 \frac{m_\ell}{m_{B_q}}$. If $m_\ell = m_e$, $m_e/m_{B_s} \sim 10^{-4}$ and thus negligible, it explains the absence of a minima in figure 5.3. The term involving C_{10} therefore never competes with C_{Q_2} in figure 5.3 as it does in figures 5.1 and 5.2.

Furthermore, the SM prediction is lower than the dark portal model in decays to electron pairs. This fact is also related to the negligible ΔC_{10} term; as it never competes with the C_{Q_2} term, the C_{Q_2} contributions dominate for all values of M_{H_1} . In short, this particular branching fraction is only enhanced in the dark portal model. Furthermore, although there are no experimental measurements of the decay mode to e^+e^- an upper bound has been set, see table 2.1. The obtained branching fraction to electron pairs in figure 5.3 is below this bound, $\mathcal{B}(B_s^0 \rightarrow e^+e^-) < 2.8 \times 10^{-7}$, at least in the convergence region.

The reason for the branching fractions converging at a specific value for large M_{H_1} could be due to that at some M_{H_1} , the propagator can be seen as pointlike, or that the perturbative calculation of the Wilson coefficients has some leading order fixed value independent of M_{H_1} and $\sin \alpha$. Further analysis of the specific diagrams leading to contributions need to be done in order to fully establish the reasons for this behaviour.

5.2 Likelihoods

The graphs depicting branching fractions as functions of M_{H_1} gave insight to the relevant contributions in different regions of the parameter space. However, the variation of $\sin \alpha$ also strongly influences the observables. Thus, scans over the two dimensional parameter space $(M_{H_1}, \sin \alpha)$ were performed using `GAMBIT`. The resulting two scans were performed using the `Diver` algorithm, see figure 5.4 and the `MultiNest` algorithm, see figure 5.5.

The scans are presented in surface plots, where the color bar corresponds to the profile likelihood ratio combining the likelihood for $\mathcal{B}(B^0 \rightarrow \mu^+\mu^-)$ and $\mathcal{B}(B_s^0 \rightarrow \mu^+\mu^-)$. The branching fraction $\mathcal{B}(B_s^0 \rightarrow e^+e^-)$ is not included as experimental measurements are absent.

From figures 5.4 and 5.5 it is clear that the `Diver` and `MultiNest` scans both agree on the parameter bounds. Only very slight deviations are seen. The overall appearance of the surface plots is related to the branching fraction shapes in figures 5.1 and 5.2. For small M_{H_1} the branching fractions rapidly increase well above the experimental value, and for larger M_{H_1} the branching fractions cross it at some point. Subsequently they approach a minimum, well below the experimental value and its uncertainty, before increasing again and converging towards a fixed value represented by the large region of intermediate profile likelihood ratio that is seen in the right parts of figures 5.4 and 5.5. Furthermore, the likelihood is intermediate

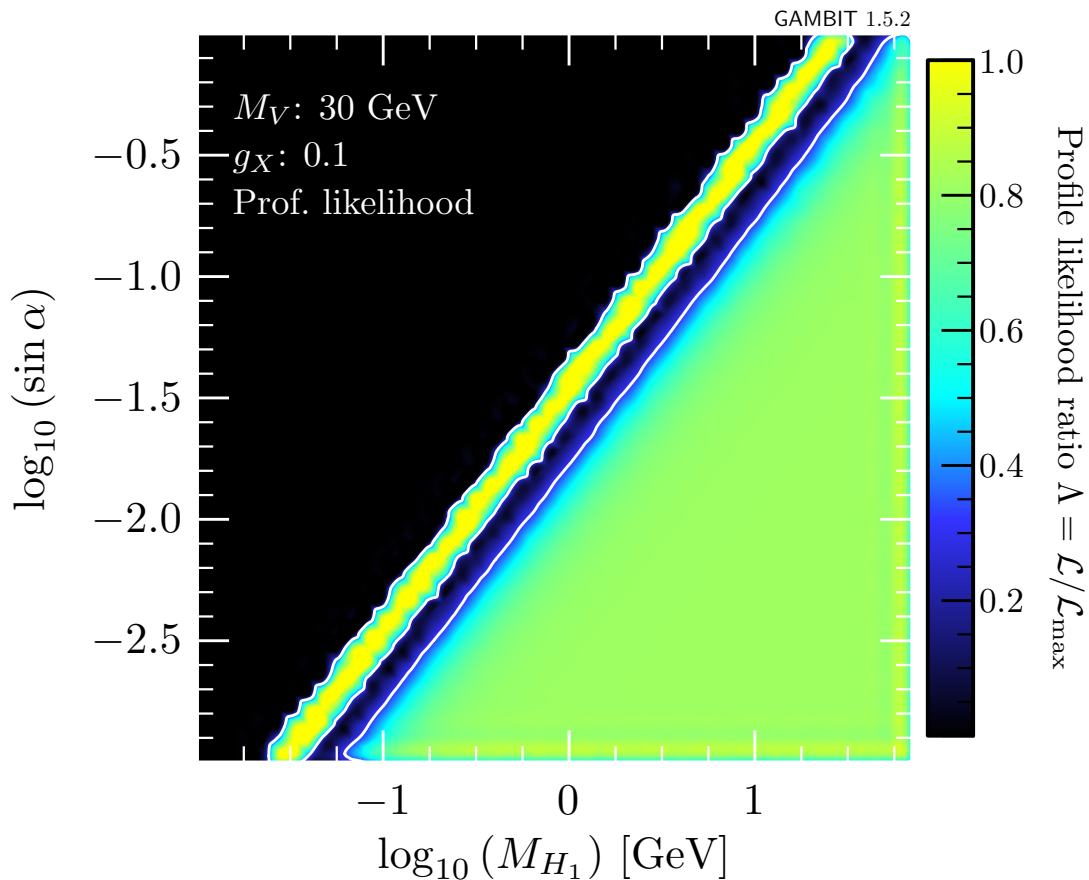


Figure 5.4: Surface plot of the combined likelihoods from branching fractions $\mathcal{B}(B_s^0 \rightarrow \mu^+\mu^-)$ and $\mathcal{B}(B^0 \rightarrow \mu^+\mu^-)$. The fundamental parameters $\sin \alpha$ and M_{H_1} were varied using the Diver scanner in GAMBIT. The white lines indicate the 68.3% confidence level. Plots were obtained using Pippi [5].

since the branching fraction $\mathcal{B}(B_s^0 \rightarrow \mu^+\mu^-)$ is within its experimental uncertainty, while $\mathcal{B}(B^0 \rightarrow \mu^+\mu^-)$ is outside its experimental uncertainty. Note that the straight line where profile likelihood is maximized has a slope corresponding roughly to $\frac{\sin^2 \alpha}{M_{H_1}^2} = 0.001$.

While it could be interesting to probe regions below $\sin \alpha = 10^{-3}$ and $M_{H_1} = 10^{-2}$ GeV, nothing suggests otherwise than a continuation of the line and the large region of flat, intermediate likelihood. The practical reason for the lower bound had however to do with computational restrictions, as the implementation suffered from numerical errors below this boundary.

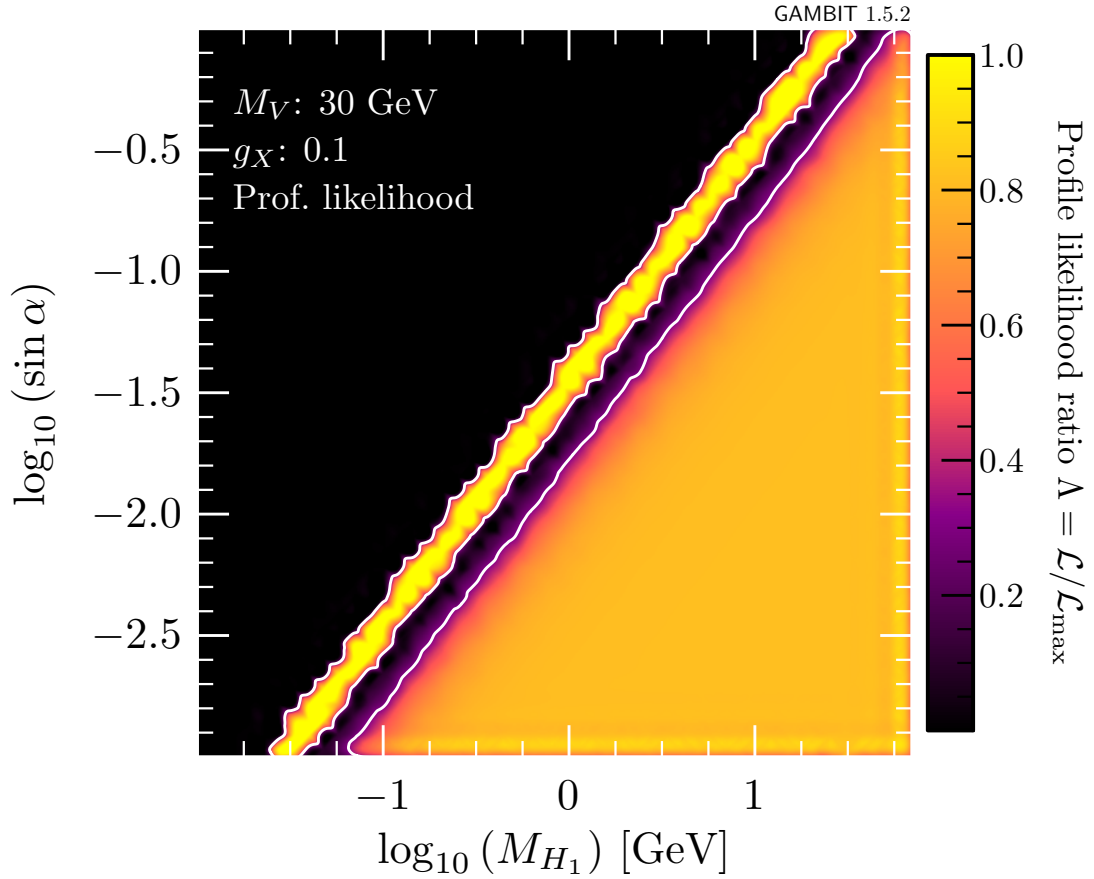


Figure 5.5: Surface plot of the combined likelihoods from branching fractions $\mathcal{B}(B_s^0 \rightarrow \mu^+\mu^-)$ and $\mathcal{B}(B^0 \rightarrow \mu^+\mu^-)$. The fundamental parameters $\sin \alpha$ and M_{H_1} were varied using the MultiNest scanner in GAMBIT. The white lines indicate the 68.3 % confidence level. Plots were obtained using Pippi [5].

6

Conclusions

I have in this work successfully implemented the full dark Higgs portal theory, brought the full theory over to the effective theory formulation where the fundamental parameters were constrained using experimental measurements of rare meson decays. The full theory was implemented in `SARAH`, the effective theory Wilson coefficients at matching scale were computed by `SPheno` and were run down to the b -quark scale using `wilson`. The observable branching fractions were computed by `SuperIso`, and scans were performed within the `GAMBIT` framework, taking place in primarily the physics module `FlavBit`. Using my implementation, I scanned the parameters M_{H_1} and $\sin \alpha$ using `GAMBIT` using three different sampling algorithms provided by `ScannerBit`.

From the resulting branching fractions as presented in figures 5.1-5.3 it is evident that for the case where the mediator mass is large and the mixing angle is small the contribution to the respective Wilson coefficients (WC) C_{Q_1} and C_{Q_2} gets heavily suppressed and the unchanged WC C_{10} starts to dominate. This behaviour does however not occur for the branching fraction $\mathcal{B}(B_s^0 \rightarrow e^+e^-)$, where the presence of C_{10} is instead heavily suppressed by B-meson mass. Instead, the tiny contribution from the suppressed C_{Q_1, Q_2} dominates in this case, explaining why the branching fraction is larger than the SM value in contrast to the case where the B-meson decays to muon pairs. For small M_{H_1} and larger mixing angles the branching fractions explode to large values incompatible with experimental measurements.

From figures 5.4-5.5 I conclude that simulations are in best agreement with results in a narrow region around a line with the slope $\sin^2 \alpha / M_{H_1}^2 = 0.001$. Below this line, there is a small region with low likelihood, consistent with the minimas seen in figures 5.1-5.2 followed by a large region of flat, intermediate likelihood that is consistent with the fact that the branching fractions converge as C_{Q_1, Q_2} are suppressed with increasing M_{H_1} . Above the line, the values are incompatible with experiments as the branching fractions gets unreasonably large.

From all performed scans including initial test runs, variation of the dark matter mass M_V and the $U(1)_X$ gauge coupling g_X made little to no impact on the resulting branching fractions. Hence, the gauge-scalar interactions (3.7) of the hidden sector do not enter at the 1-loop level of the considered flavour changing decays.

I can therefore conclude that the dark Higgs portal model is compatible with experimental results if relations between parameters are such that, roughly $\sin^2 \alpha / M_{H_1}^2 =$

0.001 where M_{H_1} is in units of GeV. Furthermore, this relation only holds for $10^{0.5} \lesssim M_{H_1} \lesssim 10^{1.5}$ GeV. For M_{H_1} larger than this, all values for $\sin \alpha$ are more or less equally probable. Variation of the parameters M_V and g_X does not influence the present analysis.

6.1 Future work

In the future, more constraining power will be available as upcoming experiments will be able to measure the branching fractions in question with smaller error bars. The hunt is still on for a conclusive signal on the $B_s^0 \rightarrow e^+e^-$ decay, which would aid in further constraining the dark Higgs portal model.

From my conclusions, being that $M_{H_1} < 10^{1.5} \approx 31.6$ GeV, the decay of the SM Higgs $H_2 \rightarrow H_1H_1$ is allowed and could account for the invisible decays of the SM Higgs either fully or together with the decay $H_2 \rightarrow VV$, possible if $M_V < M_{H_2}/2$ [35]. The model can therefore be constrained further by imposing the constraint $\mathcal{B}(H_2 \rightarrow \text{inv}) \lesssim 25\%$, combined with my results.

Being a minimal extension to the SM, the Higgs portal can be further built upon by either extending the particle content in the dark sector or by including gauge kinetic mixing. Any such additions can give further contributions to the Wilson coefficients involved in rare meson decays not only to lepton pairs, but also to the other decay channels (4.4) as computable by `FlavBit`. The strength of my implementation is that being a minimal extension, it is easy to build upon and does not require any major changes to the code as it is implemented in the `GAMBIT` framework.

Bibliography

- [1] N. Serra and T. Blake, “Chasing new physics with electroweak penguins,” May 22 2013. URL: <https://cerncourier.com/a/chasing-new-physics-with-electroweak-penguins/>. Accessed: 2021-06-14.
- [2] D. H. Rogstad and G. S. Shostak, “Gross Properties of Five Scd Galaxies as Determined from 21-CENTIMETER Observations,” *Astrophysical Journal*, vol. 176, p. 315, Sept. 1972.
- [3] Planck Collaboration, P. A. R. Ade, *et al.*, “Planck 2013 results. I. Overview of products and scientific results,” *Astronomy and Astrophysics*, vol. 571, p. A1, Nov. 2014.
- [4] J. Serrano, *Study of rare leptonic B meson decays with the LHCb experiment*. Habilitation à diriger des recherches, Aix Marseille Université, Nov. 2019.
- [5] P. Scott, “Pippi — Painless parsing, post-processing and plotting of posterior and likelihood samples,” *European Physical Journal Plus*, vol. 127, p. 138, Nov. 2012.
- [6] J. Albrecht, S. Reichert, and D. van Dyk, “Status of rare exclusive B meson decays in 2018,” *International Journal of Modern Physics A*, vol. 33, p. 1830016, July 2018.
- [7] G. Bertone and D. Hooper, “History of dark matter,” *Reviews of Modern Physics*, vol. 90, Oct 2018.
- [8] M. J. Dolan, F. Kahlhoefer, C. McCabe, and K. Schmidt-Hoberg, “A taste of dark matter: flavour constraints on pseudoscalar mediators,” *Journal of High Energy Physics*, vol. 2015, Mar 2015.
- [9] P. Schneider, *Extragalactic Astronomy and Cosmology: An Introduction*. Springer Berlin Heidelberg, 2015.
- [10] J. F. Navarro, C. S. Frenk, and S. D. M. White, “The Structure of Cold Dark Matter Halos,” *Astrophysical Journal*, vol. 462, p. 563, May 1996.
- [11] R. Massey, T. Kitching, and J. Richard, “The dark matter of gravitational lensing,” *Reports on Progress in Physics*, vol. 73, p. 086901, Aug. 2010.
- [12] I. Kovner, “The Thick Gravitational Lens: A Lens Composed of Many Elements at Different Distances,” *Astrophysical Journal*, vol. 316, p. 52, May 1987.
- [13] G. Soucail, Y. Mellier, B. Fort, G. Mathez, and M. Cailloux, “The giant arc in A 370 : spectroscopic evidence for gravitational lensing from a source at $Z=0.724$,” *Astronomy and Astrophysics*, vol. 191, pp. L19–L21, Feb. 1988.
- [14] R. S. Ellis, “Gravitational lensing: a unique probe of dark matter and dark energy,” *Philosophical Transactions of the Royal Society of London Series A*, vol. 368, pp. 967–987, Feb. 2010.

- [15] K. Garrett and G. Dūda, “Dark Matter: A Primer,” *Advances in Astronomy*, vol. 2011, p. 968283, Jan. 2011.
- [16] R. Tojeiro, “Understanding the cosmic microwave background temperature power spectrum,” 2006.
- [17] Planck Collaboration, P. A. R. Ade, *et al.*, “Planck 2013 results. XVI. Cosmological parameters,” *Astronomy and Astrophysics*, vol. 571, p. A16, Nov. 2014.
- [18] G. Arcadi, M. Dutra, P. Ghosh, M. Lindner, Y. Mambrini, M. Pierre, S. Profumo, and F. S. Queiroz, “The waning of the wimp? a review of models, searches, and constraints,” *The European Physical Journal C*, vol. 78, Mar 2018.
- [19] M. Schumann, “Direct detection of WIMP dark matter: concepts and status,” *Journal of Physics G Nuclear Physics*, vol. 46, p. 103003, Oct. 2019.
- [20] C. Pérez de los Heros, “Status, Challenges and Directions in Indirect Dark Matter Searches,” *Symmetry*, vol. 12, p. 1648, Oct. 2020.
- [21] N. F. Bell, M. J. Dolan, and S. Robles, “Searching for Sub-GeV dark matter in the galactic centre using Hyper-Kamiokande,” *Journal of Cosmology and Astroparticle Physics*, vol. 2020, p. 019, Sept. 2020.
- [22] S. Giagu, “Wimp dark matter searches with the atlas detector at the lhc,” *Frontiers in Physics*, vol. 7, p. 75, 2019.
- [23] ATLAS Collaboration, “Search for light long-lived neutral particles produced in pp collisions at $\sqrt{s} = 13$ TeV and decaying into collimated leptons or light hadrons with the ATLAS detector,” *arXiv e-prints*, p. arXiv:1909.01246, Sept. 2019.
- [24] M. Aaboud *et al.*, “Search for Higgs boson decays to beyond-the-Standard-Model light bosons in four-lepton events with the ATLAS detector at $\sqrt{s}=13$ TeV,” *Journal of High Energy Physics*, vol. 2018, p. 166, June 2018.
- [25] D. Salvatore, “Search for long-lived neutral particles decaying into Lepton-Jets with the ATLAS detector in proton-proton collision data at 13 TeV,” *arXiv e-prints*, p. arXiv:1708.07625, Aug. 2017.
- [26] Cms Collaboration, V. Khachatryan, *et al.*, “Observation of the rare $B_s^0 \rightarrow \mu^+ \mu^-$ decay from the combined analysis of CMS and LHCb data,” *Nature*, vol. 522, pp. 68–72, June 2015.
- [27] T. Aaltonen *et al.*, “Search for the Decays $B_{(s)}^0 \rightarrow e^+ \mu^-$ and $B_{(s)}^0 \rightarrow e^+ e^-$ in CDF Run II,” *Physical Review Letters*, vol. 102, p. 201801, May 2009.
- [28] R. Aaij *et al.*, “Search for the decays $B_s^0 \rightarrow \tau^+ \tau^-$ and $B^0 \rightarrow \tau^+ \tau^-$,” *Phys. Rev. Lett.*, vol. 118, p. 251802, Jun 2017.
- [29] R. Aaij *et al.*, “Measurement of the $B_s^0 \rightarrow \mu^+ \mu^-$ Branching Fraction and Effective Lifetime and Search for $B^0 \rightarrow \mu^+ \mu^-$ Decays,” *Phys. Rev. Lett.*, vol. 118, p. 191801, May 2017.
- [30] C. Gross, O. Lebedev, and Y. Mambrini, “Non-Abelian gauge fields as dark matter,” *arXiv e-prints*, p. arXiv:1505.07480, May 2015.
- [31] A. Falkowski, C. Gross, and O. Lebedev, “A second higgs from the higgs portal,” *Journal of High Energy Physics*, vol. 2015, May 2015.
- [32] K. Das and S. K. Rai, “750 GeV diphoton excess in a U(1) hidden symmetry model,” *Physical Review D*, vol. 93, p. 095007, May 2016.
- [33] F. Staub, “Sarah,” *arXiv e-prints*, p. arXiv:0806.0538, June 2008.

-
- [34] M. E. Peskin and D. V. Schroeder, *An introduction to quantum field theory*. Boulder, CO: Westview, 1995. Includes exercises.
- [35] G. Arcadi, A. Djouadi, and M. Kado, “The higgs-portal for vector dark matter and the effective field theory approach: A reappraisal,” *Physics Letters B*, vol. 805, p. 135427, Jun 2020.
- [36] L. Silvestrini, “Effective Theories for Quark Flavour Physics,” *arXiv e-prints*, p. arXiv:1905.00798, May 2019.
- [37] A. J. Buras, “Weak Hamiltonian, CP Violation and Rare Decays,” *arXiv e-prints*, pp. hep-ph/9806471, June 1998.
- [38] F. Mahmoudi and S. Neshatpour, “SuperIso v4.1: A program for calculating flavor physics observables in SM, 2HDM and supersymmetry,” *arXiv e-prints*, Nov. 2020.
- [39] F. U. Bernlochner, M. Chrzyszcz, L. A. Dal, B. Farmer, P. Jackson, A. Kvellestad, F. Mahmoudi, A. Putze, C. Rogan, and et al., “Flavbit: a gambit module for computing flavour observables and likelihoods,” *The European Physical Journal C*, vol. 77, Nov 2017.
- [40] Z. Rui, Y. Li, and Z.-J. Xiao, “Branching ratios, CP asymmetries and polarizations of $B \rightarrow \psi$ (2S) V decays,” *European Physical Journal C*, vol. 77, p. 610, Sept. 2017.
- [41] A. Fodor, “Semileptonic B decay results from early Belle II data,” *arXiv e-prints*, p. arXiv:2001.01675, Jan. 2020.
- [42] F. Staub, “SARAH 4: A tool for (not only SUSY) model builders,” *Computer Physics Communications*, vol. 185, pp. 1773–1790, June 2014.
- [43] W. Porod, F. Staub, and A. Vicente, “A flavor kit for BSM models,” *European Physical Journal C*, vol. 74, p. 2992, Aug. 2014.
- [44] W. Porod, “SPHeno, a program for calculating supersymmetric spectra, SUSY particle decays and SUSY particle production at e^+e^- colliders,” *Computer Physics Communications*, vol. 153, pp. 275–315, June 2003.
- [45] W. Porod and F. Staub, “SPHeno 3.1: extensions including flavour, CP-phases and models beyond the MSSM,” *Computer Physics Communications*, vol. 183, pp. 2458–2469, Nov. 2012.
- [46] J. Aebischer, I. Brivio, A. Celis, J. A. Evans, Y. Jiang, J. Kumar, X. Pan, W. Porod, J. Rosiek, D. Shih, F. Staub, D. M. Straub, D. van Dyk, and A. Vicente, “WCxf: An exchange format for Wilson coefficients beyond the Standard Model,” *Computer Physics Communications*, vol. 232, pp. 71–83, Nov. 2018.
- [47] G. Van Rossum and F. L. Drake, *Python 3 Reference Manual*. Scotts Valley, CA: CreateSpace, 2009.
- [48] J. Aebischer, J. Kumar, and D. M. Straub, “wilson : a Python package for the running and matching of Wilson coefficients above and below the electroweak scale,” *European Physical Journal C*, vol. 78, p. 1026, Dec. 2018.
- [49] P. Athron, C. Balazs, T. Bringmann, A. Buckley, M. Chrzyszcz, J. Conrad, J. M. Cornell, L. A. Dal, H. Dickinson, and et al., “Gambit: the global and modular beyond-the-standard-model inference tool,” *The European Physical Journal C*, vol. 77, Nov 2017.

- [50] G. D. Martinez, J. McKay, B. Farmer, P. Scott, E. Roebber, A. Putze, and J. Conrad, “Comparison of statistical sampling methods with scannerbit, the gambit scanning module,” *The European Physical Journal C*, vol. 77, Nov 2017.
- [51] W. R. Inc., “Mathematica, Version 12.1.” Champaign, IL, 2020.
- [52] A. Vicente, “Computer tools in particle physics,” *arXiv e-prints*, p. arXiv:1507.06349, July 2015.
- [53] Particle Data Group, P. A. Zyla, *et al.*, “Review of Particle Physics,” *Progress of Theoretical and Experimental Physics*, vol. 2020, p. 083C01, Aug. 2020.
- [54] “Basis eos (eft wet),” Oct. 31 2019. URL: wcof.github.io/assets/pdf/WET.EOS.pdf. Accessed: 2021-05-25.

A

Mathematical derivations

The derivations presented in this chapter are meant to fill in the calculation gaps that are present in section 3.1 and all of its subsections. For details of where and when the different results are used, see section 3.1.

A.1 Kinetic term $(D_\mu S)^\dagger(D^\mu S)$

Inserting the covariant derivative $D_\mu = \partial_\mu S - ig_X Y_X V_\mu S$ into $(D_\mu S)^\dagger(D^\mu S)$, and expanding $S = \frac{1}{\sqrt{2}}(\phi_S + v_S)$ expressed in the unitary gauge,

$$\begin{aligned}
(D_\mu S)^\dagger(D^\mu S) &= \frac{1}{2}(\partial_\mu \phi_S - ig_X Y_X V_\mu \phi_S - ig_X Y_X v_S V_\mu) \times \\
&\quad \times (\partial^\mu \phi_S + ig_X Y_X V^\mu \phi_S + ig_X Y_X v_S V^\mu) \\
&= \frac{1}{2}(\partial_\mu \phi_S \partial^\mu \phi_S + g_X^2 Y_X^2 V_\mu V^\mu \phi_S \phi_S + g_X^2 Y_X^2 v_S^2 V_\mu V^\mu - \\
&\quad + ig_X Y_X \partial_\mu \phi_S V^\mu \phi_S + ig_X Y_X v_S \partial_\mu \phi_S V^\mu - ig_X Y_X V_\mu \phi_S \partial^\mu \phi_S - \\
&\quad - ig_X Y_X v_S V_\mu \partial^\mu \phi_S + v_S g_X^2 Y_X^2 V_\mu \phi_S V^\mu + g_X^2 Y_X^2 v_S V_\mu V^\mu \phi_S) \\
&= \frac{1}{2}(\partial_\mu \phi_S \partial^\mu \phi_S + g_X^2 Y_X^2 V_\mu V^\mu \phi_S \phi_S + g_X^2 Y_X^2 v_S^2 V_\mu V^\mu + \\
&\quad + 2v_S g_X^2 Y_X^2 V_\mu V^\mu \phi_S). \tag{A.1}
\end{aligned}$$

From the above third term, the vector dark matter mass can be identified as $m_V = \sqrt{g_X^2 Y_X^2 v_S^2}$. The other terms represent the gauge-scalar interactions.

A.2 Tadpole equations

Assuming that $H = (0, \frac{\phi_H}{\sqrt{2}})$, $S = \frac{\phi_S}{\sqrt{2}}$ in the unitary gauge, the potential (3.10) can be written

$$V(H, S) = \frac{\mu_S^2 \phi_S^2}{2} + \frac{\mu_H^2 \phi_H^2}{2} + \frac{\lambda_S \phi_S^4}{4} + \frac{\lambda_H \phi_H^4}{4} + \frac{\lambda_{HS} \phi_S^2 \phi_H^2}{4}. \tag{A.2}$$

Assuming that at potential minima, ϕ_S and ϕ_H develops vacuum expectation values v_S, v_H so that $\langle \phi_{S/H} \rangle = |\phi_{S/H}| = v_{S/H}$, then

$$\left. \frac{\partial V(H, S)}{\partial |\phi_S|} \right|_{|\phi_S|=v_S} = \mu_S^2 v_S + \lambda_S v_S^3 + \frac{1}{2} \lambda_{HS} v_H^2 v_S = 0 \implies \mu_S^2 = -\lambda_S v_S^2 - \frac{1}{2} \lambda_{HS} v_H^2 \quad (\text{A.3})$$

$$\left. \frac{\partial V(H, S)}{\partial |\phi_H|} \right|_{|\phi_H|=v_H} = \mu_H^2 v_H + \lambda_H v_H^3 + \frac{1}{2} \lambda_{HS} v_S^2 v_H = 0 \implies \mu_H^2 = -\lambda_H v_H^2 - \frac{1}{2} \lambda_{HS} v_S^2. \quad (\text{A.4})$$

A.3 Mass matrix

The mass matrix

$$\mathcal{M}^2 = \begin{pmatrix} 2\lambda_S v_S^2 & \lambda_{HS} v_H v_S \\ \lambda_{HS} v_H v_S & 2\lambda_H v_H^2 \end{pmatrix} \quad (\text{A.5})$$

is positive definite if its pivots are larger than zero, since it is symmetric. Subtract the second row by the first row multiplied by $\frac{\lambda_{HS} v_H}{2\lambda_S v_S}$,

$$\mathcal{M}^2 = \begin{pmatrix} 2\lambda_S v_S^2 & \lambda_{HS} v_H v_S \\ 0 & 2\lambda_H v_H^2 - \frac{v_H^2 \lambda_{HS}^2}{2\lambda_S} \end{pmatrix} \quad (\text{A.6})$$

First, its required that the pivot $\mathcal{M}_{22}^2 > 0$. So,

$$2\lambda_H v_H^2 > \frac{v_H^2 \lambda_{HS}^2}{2\lambda_S} \quad (\text{A.7})$$

$$\implies \lambda_H > \frac{\lambda_{HS}^2}{4\lambda_S} \quad (\text{A.8})$$

where its also required that $\lambda_S > 0$, since the first pivot also needs to be positive. These two requirements are needed for the mass matrix to be positive definite.

A.4 Parameter substitutions

Using both equations in (3.17), the new relation

$$M_{H_1}^2 - M_{H_2}^2 = 2 \left(\frac{\lambda_S v_S^2 - \lambda_H v_H^2}{\cos 2\alpha} \right) \quad (\text{A.9})$$

is found. Rewriting (3.16),

$$\tan 2\alpha = \frac{\lambda_{HS} v_H v_S}{\lambda_S v_S^2 - \lambda_H v_H^2} \implies \lambda_{HS} v_H v_S = \frac{\sin 2\alpha}{2} (M_{H_1}^2 - M_{H_2}^2) \quad (\text{A.10})$$

and solving for v_S

$$v_S = \frac{\sin 2\alpha}{2\lambda_{HS} v_H} (M_{H_1}^2 - M_{H_2}^2) \quad (\text{A.11})$$

Starting with the expression for $M_{H_1}^2$ and inserting the usual relation $M_{H_1}^2 - M_{H_2}^2$

$$M_{H_1}^2 = \lambda_H v_H^2 + \lambda_S v_S^2 + \frac{M_{H_1}^2 - M_{H_2}^2}{2}. \quad (\text{A.12})$$

and, using the expression for $\lambda_S v_S^2 = \frac{M_{H_1}^2 - M_{H_2}^2}{2} \cos 2\alpha + \lambda_H v_H^2$

$$M_{H_1}^2 = 2\lambda_H v_H^2 + \frac{\cos 2\alpha}{2} (M_{H_1}^2 - M_{H_2}^2) + \frac{M_{H_1}^2 - M_{H_2}^2}{2} \quad (\text{A.13})$$

$$= 2\lambda_H v_H^2 + \frac{\cos 2\alpha + 1}{2} (M_{H_1}^2 - M_{H_2}^2) \quad (\text{A.14})$$

$$= 2\lambda_H v_H^2 + (1 - \sin^2 \alpha) (M_{H_1}^2 - M_{H_2}^2) \quad (\text{A.15})$$

$$\implies \lambda_H = \frac{M_{H_1}^2}{2v_H^2} - \frac{(1 - \sin^2 \alpha) (M_{H_1}^2 - M_{H_2}^2)}{2v_H^2} \quad (\text{A.16})$$

$$= \frac{M_{H_2}^2}{2v_H^2} + \frac{\sin^2 \alpha (M_{H_1}^2 - M_{H_2}^2)}{2v_H^2}. \quad (\text{A.17})$$

Now, consider instead the expression for $M_{H_2}^2$

$$M_{H_2}^2 = \lambda_H v_H^2 + \lambda_S v_S^2 - \frac{M_{H_1}^2 - M_{H_2}^2}{2}. \quad (\text{A.18})$$

Inserting the newly found λ_H ,

$$M_{H_2}^2 = \lambda_S v_S^2 - \left(\frac{M_{H_1}^2 - M_{H_2}^2}{2} \right) + \frac{M_{H_2}^2}{2} + \frac{\sin^2 \alpha (M_{H_1}^2 - M_{H_2}^2)}{2} \quad (\text{A.19})$$

$$\implies \lambda_S v_S^2 = \frac{M_{H_1}^2}{2} - \frac{\sin^2 \alpha}{2} (M_{H_1}^2 - M_{H_2}^2) \quad (\text{A.20})$$

Inserting the expression for v_S and dividing both sides by it,

$$\lambda_S = \frac{4\lambda_{HS}^2 v_H^2}{(M_{H_1}^2 - M_{H_2}^2)^2 \sin^2 2\alpha} \left(\frac{M_{H_1}^2}{2} - \frac{\sin^2 \alpha}{2} (M_{H_1}^2 - M_{H_2}^2) \right) \quad (\text{A.21})$$

$$= \frac{4\lambda_{HS}^2 v_H^2}{(M_{H_1}^2 - M_{H_2}^2)^2 \sin^2 2\alpha} (M_{H_1}^2 - M_{H_2}^2) \left(\frac{M_{H_1}^2}{2(M_{H_1}^2 - M_{H_2}^2)} - \frac{\sin^2 \alpha}{2} \right) \quad (\text{A.22})$$

$$= \frac{2\lambda_{HS}^2 v_H^2}{(M_{H_1}^2 - M_{H_2}^2) \sin^2 2\alpha} \left(\frac{M_{H_1}^2}{M_{H_1}^2 - M_{H_2}^2} - \sin^2 \alpha \right). \quad (\text{A.23})$$

Hence, the free parameters $(v_S, v_H, \lambda_H, \lambda_{HS}, \lambda_S)$ can be traded the set $(M_{H_1}, M_{H_2}, \sin \alpha, v_H, \lambda_{HS})$ by the relations

$$\lambda_H = \frac{M_{H_2}^2}{2v_H^2} + \frac{\sin^2 \alpha (M_{H_1}^2 - M_{H_2}^2)}{2v_H^2} \quad (\text{A.24})$$

$$\lambda_S = \frac{2\lambda_{HS}^2 v_H^2}{(M_{H_1}^2 - M_{H_2}^2) \sin^2 2\alpha} \left(\frac{M_{H_1}^2}{M_{H_1}^2 - M_{H_2}^2} - \sin^2 \alpha \right) \quad (\text{A.25})$$

$$v_S = \frac{\sin(2\alpha)}{2\lambda_{HS} v_H} (M_{H_1}^2 - M_{H_2}^2) \quad (\text{A.26})$$

A. Mathematical derivations

Another trade is also possible: consider using the relation $M_{H_1}^2 - M_{H_2}^2$, multiplying both sides by $\sin 2\alpha$

$$\sin 2\alpha(M_{H_1}^2 - M_{H_2}^2) = 2(\lambda_S v_S^2 - \lambda_H v_H^2) \tan 2\alpha = 2\lambda_{HS} v_H v_S \quad (\text{A.27})$$

and rearranging,

$$\lambda_{HS} = \frac{\sin 2\alpha(M_{H_1}^2 - M_{H_2}^2)}{2v_H v_S}. \quad (\text{A.28})$$

Inserting another equation for v_S namely $g_X^2 = 4M_V^2/v_S^2$, the above expression becomes

$$\lambda_{HS} = \frac{\sin 2\alpha(M_{H_1}^2 - M_{H_2}^2)g_X}{4M_V v_H} \quad (\text{A.29})$$

Inserting λ_{HS} into the expression for λ_S ,

$$\lambda_S = \left(\frac{\sin^2 2\alpha(M_{H_1}^2 - M_{H_2}^2)^2 g_X^2}{16M_V^2 v_H^2} \right) \frac{2v_H^2}{(M_{H_1}^2 - M_{H_2}^2) \sin^2 2\alpha} \left(\frac{M_{H_1}^2}{M_{H_1}^2 - M_{H_2}^2} - \sin^2 \alpha \right) \quad (\text{A.30})$$

$$= \frac{g_X^2}{8M_V^2} (M_{H_1}^2 - (M_{H_1}^2 - M_{H_2}^2) \sin^2 \alpha) \quad (\text{A.31})$$

and so the free parameters

$$(v_S, v_H, \lambda_H, \lambda_{HS}, \lambda_S)$$

can be traded for the set

$$(M_{H_1}, M_{H_2}, \sin \alpha, v_H, g_X, M_V)$$

via the relations

$$v_S = \frac{2M_V}{g_X} \quad (\text{A.32})$$

$$\lambda_H = \frac{M_{H_2}^2}{2v_H^2} + \frac{\sin^2 \alpha (M_{H_1}^2 - M_{H_2}^2)}{2v_H^2} \quad (\text{A.33})$$

$$\lambda_S = \frac{g_X^2}{8M_V^2} (M_{H_1}^2 - \sin^2 \alpha (M_{H_1}^2 - M_{H_2}^2)) \quad (\text{A.34})$$

$$\lambda_{HS} = \frac{\sin 2\alpha (M_{H_1}^2 - M_{H_2}^2) g_X}{4M_V v_H}. \quad (\text{A.35})$$

B

Computer cluster setups

Procedures for building GAMBIT on C3SE's computer cluster Vera as well as NSC's cluster Tetralith are presented in the following chapter. In this thesis, initial tests were performed on Tetralith while the results were obtained using Vera. GAMBIT version 1.5.2, SPheno version 4.0.4 and wilson version 2.1 were used.

B.1 Vera

First, load the modules and install wilson by

```
> ml foss/2019b PyYAML Eigen CMake Boost GSL SciPy-bundle
> ml dill CastXML HDF5/1.10.5-serial h5py/2.10.0-serial-Python-3.7.4
> pip install wilson
```

Then, clone the GAMBIT github repository. Add the file WCVectorDM.cpp to folder

```
/Models/src/models
```

and the file WCVectorDM.hpp to

```
/Models/include/gambit/Models/models
```

You can also add the file WCVectorDM.yaml to /yaml_files. Finally, add the translate.py to the GAMBIT root directory.

Now, cd to the root directory and make a new directory named build. In this new directory, execute the commands

```
> cmake -DWITH_MPI=ON -DBUILD_FS_MODELS=all
-Ditch="Mathematica" -DWITH_HEPMC=ON
-DEIGEN3_INCLUDE_DIR=/apps/Vera/software/Core/Eigen/3.3.7/include ..
> make -j1 scanners
> cmake ..
> make -jn gambit
```

where n is the number of cores you want to use to build GAMBIT. Once completed, build the backends by

```
> make -j1 alterbbn capgen ddcalc darkages darksusy_all_models feynhiggs
higgsbounds higgssignals micromegas montepythonlike multimodecode
spheno susyhit superiso classy gamlike nulike
```

cd back to the GAMBIT root, and check that everything compiled successfully with

```
> ./gambit backends
> ./gambit scanners
> ./gambit models
```

If everything is fine, you are good to go. Note that the GAMBIT files in appendix C.3.1-C.3.3 are built towards the temporary directories of the node(s) that the Vera job runs on, so the results needs to be copied over before exiting the job. Several paths in these files also point to specific user paths, and needs to be revised before building GAMBIT. The SPheno program used by `WCVectorDM.cpp` is compiled as standalone, outside of the GAMBIT framework. For instructions on how to build the SPheno executable, see section 4.3.

B.2 Tetralith

For installation of GAMBIT on NSC's Tetralith, load the following modules, manually install `wilson` and clone the GAMBIT github repository:

```
> module load buildenv-gcc/2018a-eb
> module load buildtool-easybuild/.4.0.1-nsc4b89db2
> module load GCCcore/6.4.0
> module load Eigen/3.3.7-nsc1
> module load icc/.2018.1.163-GCC-6.4.0-2.28
> module load impi/.2018.1.163
> module load CMake/3.19.2
> module load Boost/1.65.1-nsc1
> module load pkg-config/0.29-nsc1
> module load Python/3.6.7-nsc1
> module load PyYAML/3.12-Python-3.6.7-nsc1
> module load GSL/2.4-nsc1
> module load mathematica/12.0.0-nsc1
> module load cURL/7.69.1-nsc1
> module load netCDF-HDF5/4.7.4-1.10.6-nsc1-serial-gcc-2018a-eb

> pip install wilson

> cd /home/x_$(USER)/Gambit
> git clone $(GAMBIT_REPO)
```

Then follow the steps described in the Vera build, with the exception that you use the `cmake` command

```
> cmake -DWITH_MPI=ON -DBUILD_FS_MODELS=all -Ditch="Mathematica"  
-DWITH_HEPMC=ON ..
```

Also note that the files `WCVectorDM.cpp`, `WCVectorDM.hpp` and `WCVectorDM.yaml` are built against the Vera allocated nodes temporary directory gained when submitting a job, and to the specific home directory of the user. For doing the same on Tetralith, all these paths need to be revised.

C

Source code

This chapter serves as a collection of all source code written during the work of the thesis. The **SARAH** code is standalone, and used to generate **SPheno** modules. Compiling these modules into a **SPheno** program for the model, an executable **SPhenoVDM** is created. Together with `translate.py`, **SPhenoVDM** is used by the translation function `WCVectorDM.cpp`. Note that all paths present in `WCVectorDM.cpp` needs to be set appropriately, depending on the environment users build **GAMBIT** in. Included is also a sample **YAML** file used to run **GAMBIT** with.

C.1 SARAH

Presented below is the four files that is needed in order to use the model in **SARAH**.

C.1.1 VDM.m

The main model file.

```
1 Off[General::spell]
2
3
4 ModelName = "VDM";
5 ModelNameLaTeX = "hidden_U(1)_VDM_model";
6 ModelAuthors = "E. AAstrand (based_on_hidden_U(1)_model_by_F
   . Staub, M.E. Krauss)";
7 ModelDate = "2021-04-26";
8
9
10 (* using the model introduced in 1512.07789 *)
11 (* underlying basic model: B-L-SM *)
12 (* adapted for Higgs dark portal model 2021-04-26 *)
13
14 (*-----*)
15 (* Particle Content*)
16 (*-----*)
17
18 (* Gauge Superfields *)
19
20 Gauge[[1]] = {B, U[1], hypercharge, g1, False};
```

```

21 Gauge[[2]]={WB, SU[2], left, g2, True};
22 Gauge[[3]]={G, SU[3], color, g3, False};
23 Gauge[[4]]={Bp, U[1], chargeX, gX, False};
24
25
26 (* Chiral Superfields *)
27
28 FermionFields[[1]] = {q, 3, {uL, dL}, 1/6, 2, 3, 0};
29 FermionFields[[2]] = {l, 3, {vL, eL}, -1/2, 2, 1, 0};
30 FermionFields[[3]] = {d, 3, conj[dR], 1/3, 1, -3, 0};
31 FermionFields[[4]] = {u, 3, conj[uR], -2/3, 1, -3, 0};
32 FermionFields[[5]] = {e, 3, conj[eR], 1, 1, 1, 0};
33
34 ScalarFields[[1]] = {H, 1, {H0, Hm}, -1/2, 2, 1, 0};
35 ScalarFields[[2]] = {s1, 1, S1, 0, 1, 1, 1/2};
36
37 (*-----*)
38 (* DEFINITION *)
39 (*-----*)
40
41 NameOfStates={GaugeES, EWSB};
42
43 (* ----- Before EWSB ----- *)
44
45 DEFINITION[GaugeES][Additional]= {
46     {LagHC, {AddHC->True}},
47     {LagNoHC, {AddHC->False}}
48 };
49
50 LagNoHC = - muH2 conj[H].H - muS12 conj[s1].s1 - lamH conj[H
    ].H.conj[H].H - lamHS1 conj[H].H.conj[s1].s1 - lamS1
    conj[s1].s1.conj[s1].s1;
51
52 LagHC = - (+ Yd H.d.q + Ye H.e.l + Yu conj[H].u.q);
53
54
55 (* Gauge Sector *)
56
57 DEFINITION[EWSB][GaugeSector] =
58 {
59     {{VB,VWB[3], VBp}, {VP, VZp, VZ}, ZZ},
60     {{VWB[1], VWB[2]}, {VWm, conj[VWm]}, ZW}
61 };
62
63
64

```

```

65 (* ——— VEVs ——— *)
66
67 DEFINITION [EWSB] [VEVs]=
68 { {H0, {vH, 1/Sqrt[2]}, {sigmaH, \[ImaginaryI]/Sqrt[2]}, {
69   phiH, 1/Sqrt[2]}},
70   {S1, {vS, 1/Sqrt[2]}, {sigmaS, \[ImaginaryI]/Sqrt[2]}, {
71     phiS, 1/Sqrt[2]}}
72 };
73
74 DEFINITION [EWSB] [MatterSector]=
75 {
76   {{phiS, phiH}, {hh, ZH}},
77   {{sigmaS, sigmaH}, {Ah, ZA}},
78   {{{dL}, {conj[dR]}}}, {{DL, Vd}, {DR, Ud}},
79   {{{uL}, {conj[uR]}}}, {{UL, Vu}, {UR, Uu}},
80   {{{eL}, {conj[eR]}}}, {{EL, Ve}, {ER, Ue}}
81 };
82
83 (*—————*)
84 (* Dirac-Spinors *)
85 (*—————*)
86
87 DEFINITION [EWSB] [DiracSpinors]={
88   Fd ->{ DL, conj[DR]},
89   Fe ->{ EL, conj[ER]},
90   Fu ->{ UL, conj[UR]},
91   Fv ->{ vL, 0}};
92
93 DEFINITION [EWSB] [GaugeES]={
94   Fd1 ->{ FdL, 0},
95   Fd2 ->{ 0, FdR},
96   Fu1 ->{ Fu1, 0},
97   Fu2 ->{ 0, Fu2},
98   Fe1 ->{ Fe1, 0},
99   Fe2 ->{ 0, Fe2}};

```

C.1.2 parameters.m

The file defining all parameters in the model.

```

1 ParameterDefinitions = {
2
3 {g1,          {Description -> "Hypercharge-Coupling"}},
4
5 {g1X,        {Description -> "Mixed_Gauge_Coupling_2",

```

```

6           LesHouches -> {gauge, 10},
7           LaTeX -> "g_{YX}",
8           OutputName -> gYX}},
9 {gX1,     {Description -> "MixedGaugeCoupling1",
10          LesHouches -> {gauge, 11},
11          LaTeX -> "g_{XY}",
12          OutputName -> gXY}},
13
14 (* {g1p,   { Description -> "B-L-Coupling"}}, *)
15
16 {gX,      {Description -> "chargeX-Coupling",
17          LaTeX -> "g_{X}",
18          Dependence -> None,
19          LesHouches -> {gauge, 4},
20          OutputName -> gX }},
21
22 {MZp,     { Description -> "Z' mass"}},
23
24
25 {g2,      { Description -> "Left-Coupling"}},
26 {g3,      { Description -> "Strong-Coupling"}},
27 {AlphaS, {Description -> "AlphaStrong"}},
28 {e,       { Description -> "electric charge"}},
29 {Gf,      { Description -> "Fermi's constant"}},
30 {aEWinv,  { Description -> "inverse weak coupling constant
31           at mZ"}},
32
33 {Yu,      { Description -> "Up-Yukawa-Coupling",
34           DependenceNum -> Sqrt[2]/vH* {{
35           Mass[Fu,1], 0, 0}, {0, Mass[Fu
36           ,2], 0}, {0, 0, Mass[Fu,3]}}} },
37
38 {Yd,      { Description -> "Down-Yukawa-Coupling",
39           DependenceNum -> Sqrt[2]/vH* {{
40           Mass[Fd,1], 0, 0}, {0, Mass[Fd
41           ,2], 0}, {0, 0, Mass[Fd,3]}}} },
42
43 {Ye,      { Description -> "Lepton-Yukawa-Coupling",
44           DependenceNum -> Sqrt[2]/vH* {{
45           Mass[Fe,1], 0, 0}, {0, Mass[Fe
46           ,2], 0}, {0, 0, Mass[Fe,3]}}} },
47
48 {Mu,      { Description -> "SM Mu Parameter"}},
49 {\[Lambda], { Description -> "SM Higgs Selfcouplings"}},

```

```

45
46 {vH,          { Description -> "EW-VEV",
47               Dependence -> None,
48               DependenceOptional -> None,
49               DependenceNum -> None,
50               DependenceSPheno -> None }},
51
52
53 {ThetaW,      { Description -> "Weinberg-Angle" }},
54 {ThetaWp,     { Description -> "Theta'", DependenceNum -> None,
55               DependenceNum -> None }},
56
57 {ZZ, {Description -> "Photon-Z-Z' Mixing Matrix"}},
58 {ZW, {Description -> "W Mixing Matrix"}},
59
60 {vS,          { LaTeX -> "v_{S}",
61               Dependence -> None,
62               OutputName -> vS,
63               Real -> True,
64               LesHouches -> {VDM,1} }},
65
66 {lamH, {OutputName -> lamH,
67         LaTeX -> "\\lambda_{H}",
68         LesHouches -> {VDM,2}}},
69
70 {lamHS1, {OutputName -> lamHS1,
71          LaTeX -> "\\lambda_{HS1}",
72          LesHouches -> {VDM,3}}},
73
74 {lamS1, {OutputName -> lamS1,
75         LaTeX -> "\\lambda_{S1}",
76         LesHouches -> {VDM,4}}},
77
78 {muH2, {OutputName -> muH2,
79         LaTeX -> "\\mu_{H}^2",
80         LesHouches -> {VDM,5}}},
81
82
83 {muS12, {OutputName -> muS12,
84         LaTeX -> "\\mu_{S1}^2",
85         LesHouches -> {VDM,6}}},
86
87 {mH2, {OutputName -> mH2,
88        LaTeX -> "m^2_H",
89        LesHouches -> {VDM,7}}},
90

```

```

91 {Vu,      {Description ->"Left-Up-Mixing-Matrix"}},
92 {Vd,      {Description ->"Left-Down-Mixing-Matrix"}},
93 {Uu,      {Description ->"Right-Up-Mixing-Matrix"}},
94 {Ud,      {Description ->"Right-Down-Mixing-Matrix"}},
95 {Ve,      {Description ->"Left-Lepton-Mixing-Matrix"}},
96 {Ue,      {Description ->"Right-Lepton-Mixing-Matrix"}},
97
98 {\[Alpha], {Description ->"Scalar□mixing□angle",
99             Dependence ->None,
100            DependenceOptional ->None,
101            DependenceNum ->None,
102            DependenceSPHeno ->ArcTan[lamHS1 vS vH / (
103                                     lamS1 vS^2 - lamH vH^2)]/2 }},
104 {ZH,      {Description ->"Scalar-Mixing-Matrix",
105            DependenceOptional ->None,
106            DependenceNum ->None,
107            Dependence ->{{Cos\[Alpha], -Sin\[
108                                     Alpha]}}},
109                                     {Sin\[Alpha], Cos\[
110                                     Alpha]}}},
111
112 {ZA,      {Description ->"Pseudo-Scalar-Mixing-Matrix",
113            Dependence ->None,
114            DependenceOptional ->None,
115            DependenceNum ->None }}

```

C.1.3 particles.m

The file defining all particles in the model.

```

1
2
3 ParticleDefinitions[GaugeES] = {
4     {H0, {
5         PDG -> 0,
6         Width -> 0,
7         Mass -> Automatic,
8         FeynArtsNr -> 1,
9         LaTeX -> "H^0",
10        OutputName -> "H0" }},
11
12     {Hp, {
13         PDG -> 0,
14         Width -> 0,
15         Mass -> Automatic,

```

```

16         FeynArtsNr -> 2,
17         LaTeX -> "H^+",
18         OutputName -> "Hp" }},
19
20     {S1, {   PDG -> 0,
21             Width -> 0,
22             Mass -> Automatic,
23             FeynArtsNr -> 98,
24             LaTeX -> "S_1",
25             OutputName -> "S1" }},
26
27     {VB,    { Description -> "B-Boson" }},
28     {VG,    { Description -> "Gluon" }},
29     {VWB,   { Description -> "W-Bosons" }},
30     {gB,    { Description -> "B-Boson_Ghost" }},
31     {gG,    { Description -> "Gluon_Ghost" }},
32     {gWB,   { Description -> "W-Boson_Ghost" }}
33
34     };
35
36 ParticleDefinitions [EWSB] = {
37
38     {hh      , { Description -> "Higgs",
39                PDG -> {35,25},
40                Width -> Automatic,
41                Mass -> LesHouches,
42                FeynArtsNr -> 1,
43                LaTeX -> "h",
44                OutputName -> "h" }},
45
46     {Ah      , { Description -> "Pseudo-Scalar_Higgs",
47                PDG -> {0,0},
48                Width -> {0, External},
49                Mass -> LesHouches,
50                FeynArtsNr -> 2,
51                LaTeX -> "A^0",
52                OutputName -> "Ah" }},
53
54
55     {Hm,     { Description -> "Charged_Higgs",
56                PDG -> {0},
57                Width -> 0,
58                Mass -> LesHouches,
59                FeynArtsNr -> 3,
60                LaTeX -> "H^-",
61                OutputName -> "Hm" }},

```

```

62
63     {VP,    { Description -> "Photon" }},
64     {VZ,    { Description -> "Z-Boson",
65              Goldstone -> Ah[1] }},
66     {VG,    { Description -> "Gluon" }},
67     {VWm,   { Description -> "W-Boson",
68              Goldstone->Hm }},
69     {gP,    { Description -> "Photon_Ghost" }},
70     {gWm,   { Description -> "Negative_W-Boson_Ghost" }},
71     {gWmC,  { Description -> "Positive_W-Boson_Ghost" }},
72     {gZ,    { Description -> "Z-Boson_Ghost" }},
73     {gG,    { Description -> "Gluon_Ghost" }},
74     {VZp,   { Description -> "Z'-Boson",
75              Goldstone -> Ah[2] }},
76     {gZp,   { Description -> "Z'-Ghost" }},
77
78
79     {Fd,    { Description -> "Down-Quarks" }},
80     {Fu,    { Description -> "Up-Quarks" }},
81     {Fe,    { Description -> "Leptons" }},
82     {Fv,    { Description -> "Neutrinos" }}
83
84     };
85
86 WeylFermionAndIndermediate = {
87
88     {H,      { PDG -> 0,
89              Width -> 0,
90              Mass -> Automatic,
91              LaTeX -> "H",
92              OutputName -> "" }},
93
94     {s1,     { PDG -> 0,
95              Width -> 0,
96              Mass -> Automatic,
97              LaTeX -> "s_1",
98              OutputName -> "" }},
99
100    {phiS,    { LaTeX -> "\\phi_{S}" }},
101    {phiH,    { LaTeX -> "\\phi_{H}" }},
102    {sigmaS,  { LaTeX -> "\\sigma_{S}" }},
103    {sigmaH,  { LaTeX -> "\\sigma_{H}" }},
104
105
106    {dR,      {LaTeX -> "d_R" }},
107    {eR,      {LaTeX -> "e_R" }}

```

```

108   {lep ,      {LaTeX -> "l" }},
109   {uR,      {LaTeX -> "u_R" }},
110   {q,      {LaTeX -> "q" }},
111   {eL,      {LaTeX -> "e_L" }},
112   {dL,      {LaTeX -> "d_L" }},
113   {uL,      {LaTeX -> "u_L" }},
114   {vL,      {LaTeX -> "\\nu_L" }},
115   {xqL,     {LaTeX -> "xq_L" }},
116   {xqR,     {LaTeX -> "xq_R" }},
117
118   {DR,      {LaTeX -> "D_R" }},
119   {ER,      {LaTeX -> "E_R" }},
120   {UR,      {LaTeX -> "U_R" }},
121   {EL,      {LaTeX -> "E_L" }},
122   {DL,      {LaTeX -> "D_L" }},
123   {UL,      {LaTeX -> "U_L" }}
124   };

```

C.1.4 SPheno.m

The file specifying the generation of **SPheno** modules.

```

1  OnlyLowEnergySPheno = True;
2
3
4  MINPAR={{1,LambdaHINPUT},
5          {2,LambdaHS1INPUT},
6          {4,LambdaS1INPUT},
7          {5, gXINPUT},
8          {6, g1XINPUT},
9          {7, vSINPUT},
10         {8, vHINPUT}};
11
12  ParametersToSolveTadpoles = {muS12,muH2};
13
14  DEFINITION[MatchingConditions]= {
15   {vH, vSM},
16   {Ye, YeSM},
17   {Yd, YdSM},
18   {Yu, YuSM},
19   {g1, g1SM},
20   {g2, g2SM},
21   {g3, g3SM}
22  };
23
24
25  BoundaryLowScaleInput={

```

```
26 {gX,gXINPUT},
27 {g1X,g1XINPUT},
28 {gX1,0},
29 {lamH, LambdaHINPUT},
30 {lamHS1, LambdaHS1INPUT},
31 {lamS1, LambdaS1INPUT},
32 {vS,vSINPUT},
33 {vH,vHINPUT}
34 };
35
36
37
38 ListDecayParticles = {Fu,Fe,Fd,hh,VZp};
39 ListDecayParticles3B = {{Fu,"Fu.f90"},{Fd,"Fd.f90"}};
40
41 DEFINITION[MatchingConditions]=Default[OHDM];
42
43
44 DefaultInputValues ={LambdaHINPUT -> 0.85,
45                      LambdaS1INPUT -> 0.1,
46                      LambdaHSINPUT1 -> 0.03
47                      gXINPUT -> 0.5,
48                      vSINPUT -> 200,
49                      vHINPUT -> 246.22,
50                      g1XINPUT -> 0};
```

C.2 translate.py

This is the auxiliary function that performs translation and running of the numerical Wilson coefficients. It requires the package `wilson`, and outputs the relevant WCs to a text-file.

```
1 import sys
2 import numpy as np
3 from wilson import Wilson
4
5 filenameIN = sys.argv[-1]
6
7 with open(filenameIN) as f:
8     params = Wilson.load_wc(f)
9
10 wc = params.match_run(scale =4.18, eft ="WEI", basis ="EOS")
11
12 original_stdout = sys.stdout # Save a reference to the
13     original standard output
```

```

14 filenameout = filenameIN+"-out"+" .txt "
15
16 with open(filenameout , 'w') as f:
17     sys.stdout = f # Change the standard output to the file
18                     created file .
19
20     print ("Re(c1)␣",wc["b->s::c1"].real)
21     print ("Re(c2)␣",wc["b->s::c2"].real)
22     print ("Re(c3)␣",wc["b->s::c3"].real)
23     print ("Re(c4)␣",wc["b->s::c4"].real)
24     print ("Re(c5)␣",wc["b->s::c5"].real)
25     print ("Re(c6)␣",wc["b->s::c6"].real)
26     print ("Re(c7)␣",wc["b->s::Re{c7}"].real)
27     print ("Im(c7)␣",wc["b->s::Im{c7}"].real)
28     print ("Re(c7')␣",wc["b->s::Re{c7'}"].real)
29     print ("Im(c7')␣",wc["b->s::Im{c7'}"].real)
30     print ("Re(c8)␣",wc["b->s::c8"].real)
31     print ("Re(c8')␣",wc["b->s::c8'"].real)
32     print ("Re(c9)␣",wc["b->see::Re{c9}"].real)
33     print ("Im(c9)␣",wc["b->see::Im{c9}"].real)
34     print ("Re(c9')␣",wc["b->see::Re{c9'}"].real)
35     print ("Im(c9')␣",wc["b->see::Im{c9'}"].real)
36     print ("Re(c10)␣",wc["b->see::Re{c10}"].real)
37     print ("Im(c10)␣",wc["b->see::Im{c10}"].real)
38     print ("Re(c10')␣",wc["b->see::Re{c10'}"].real)
39     print ("Im(c10')␣",wc["b->see::Im{c10'}"].real)
40     print ("Re(cQ1)␣",wc["b->see::Re{cS}"].real)
41     print ("Im(cQ1)␣",wc["b->see::Im{cS}"].real)
42     print ("Re(cQ1')␣",wc["b->see::Re{cS'}"].real)
43     print ("Im(cQ1')␣",wc["b->see::Im{cS'}"].real)
44     print ("Re(cQ2)␣",wc["b->see::Re{cP}"].real)
45     print ("Im(cQ2)␣",wc["b->see::Im{cP}"].real)
46     print ("Re(cQ2')␣",wc["b->see::Re{cP'}"].real)
47     print ("Im(cQ2')␣",wc["b->see::Im{cP'}"].real)
48
49     sys.stdout = original_stdout # Reset the standard output
50                                     to its original value
51
52 print("Complete. ")

```

C.3 GAMBIT

Below are the two GAMBIT model files that needs to be included when building GAMBIT. The last file is a sample YAML file, that initiates a scan and outputs the computed observables to a HDF5 file.

C.3.1 WCVectorDM.hpp

The model definition in GAMBIT.

```
1 #include "gambit/Models/models/WC.hpp"
2
3 #ifndef __WCVectorDM_hpp__
4 #define __WCVectorDM_hpp__
5
6 #define MODEL WCVectorDM
7 #define PARENT WC
8 START_MODEL
9 DEFINEPARS(M1,M2,sinTheta ,vH,gX,MV)
10 INTERPRET_AS_PARENT_FUNCTION(WCVectorDM_to_WC)
11 // Translation functions defined in WCVectorDM.cpp
12
13 #undef PARENT
14 #undef MODEL
15
16 #endif
```

C.3.2 WCVectorDM.cpp

The translation function used by the above model definition. Requires the routines `translate.py` from C.2 and the `SPhenoVDM` compiled using the output from `SARAH`. Note that the paths on lines 40 to 66 needs to be set according to the users conventions.

```
1 #include "gambit/Models/model_macros.hpp"
2 #include "gambit/Models/models/WCVectorDM.hpp"
3 #include <stdio.h>
4 #include <string.h>
5 #include <stdlib.h>
6 #include <string>
7
8 #define MODEL WCVectorDM
9 #define PARENT WC
10 #define MAX 256
11 #define STRPAR 20
12 #define PLEN 2000
13
14 // function definition
15 void MODEL_NAMESPACE::WCVectorDM_to_WC(const ModelParameters
    & VDMparams, ModelParameters& parentparams) {
16     double M1 = VDMparams["M1"];
17     double M2 = VDMparams["M2"];
18     double sinTheta = VDMparams["sinTheta"];
19     double VH = VDMparams["vH"];
```

```

20  double GX = VDMparams[ "gX" ];
21  double MV = VDMparams[ "MV" ];
22
23  double LH, LHS, LS, VS;
24
25  VS = 2*MV/GX;
26  LH = M2*M2/(2*VH*VH)+sinTheta*sinTheta*(M1*M1 - M2*M2)/(2*
    VH*VH);
27  LS = GX*GX/(8*MV*MV)*(M1*M1-sinTheta*sinTheta*(M1*M1-M2*M2
    ));
28  LHS = 2*sinTheta*cos( asin( sinTheta ) )*(M1*M1-M2*M2)*GX/(4*
    MV*VH);
29
30  // File declarations: read LesHouches, write temp, read
    output
31  FILE *fp1, *fp2;
32  // Line numbers corresponding to parameters in LesHouches
    to be replaced
33  int lno1 = 13, lno2=14, lno3 = 15, lno4 = 16, lno5 = 18,
    lno6 = 19;
34
35  int linectr = 0;
36  char str [MAX];
37  char newLH [MAX]=" ", newLHS [MAX]=" ", newLS [MAX]=" ";
38  char newGX [MAX]=" ", newVS [MAX]=" ", newVH [MAX]=" ";
39
40  // Get TMPDIR path
41  std::string TMPDIR = getenv("TMPDIR");
42
43  // Set File paths //
44  char tempPath [PLEN];
45  strcpy(tempPath, TMPDIR.c_str());
46  strcat(tempPath, "/temp_");
47
48  char outputPath [PLEN];
49  strcpy(outputPath, TMPDIR.c_str());
50  strcat(outputPath, "/VDMoutput_");
51
52  char wcPath [PLEN];
53  strcpy(wcPath, TMPDIR.c_str());
54  strcat(wcPath, "/WCS_");
55
56  char tempLHpath [PLEN];
57  strcpy(tempLHpath, TMPDIR.c_str());
58  strcat(tempLHpath, "/LesHouches.in.VDM_");
59

```

```
60  char outputWC [PLEN]      = " ";
61  char lesHouchesPath [PLEN] = "/cephyr/users/$USER/Vera/
    SPheno-4.0.4/VDM/Input_Files/LesHouches.in.VDM";
62
63  // Paths to exes //
64  char execCMD [PLEN]      = "/cephyr/users/$USER/Vera/
    SPheno-4.0.4/bin/SPhenoVDM";
65  char execTranslate [PLEN] = "python3_/cephyr/users/$USER/
    Vera/gambit_1.5/translate.py_";
66  char cpCMD [PLEN]        = "cp_";
67  //
68
69  // Make combination unique so that threads dont try to
    read/write/run same files
70  double combo = M1*100+MV+GX*10+sinTheta*10;
71  char strComb [STRPAR];
72  sprintf (strComb, "%.10f", combo);
73
74  // Make temporary file unique
75  strcat (tempPath, strComb);
76
77  // Make SPheno output file unique
78  strcat (outputPath, strComb);
79
80  // Make SPheno WC output file unique
81  strcat (wcPath, strComb);
82  strcat (execTranslate, wcPath);
83
84  // This string corresponds to WC file after translation
85  strcat (outputWC, wcPath);
86  strcat (outputWC, "-out.txt");
87
88  // Copy a temporary unique LesHouches to read from
89  strcat (tempLHpath, strComb);
90  strcat (cpCMD, lesHouchesPath);
91  strcat (cpCMD, "_");
92  strcat (cpCMD, tempLHpath);
93
94  system (cpCMD);
95
96  // The command to run SPheno is /SPHENODIR IN OUT OUTWC
97  strcat (execCMD, "_");
98  strcat (execCMD, tempPath);
99  strcat (execCMD, "_");
100  strcat (execCMD, outputPath);
101  strcat (execCMD, "_");
```

```

102  strcat(execCMD,wcPath);
103
104  // In order to remove the temporary files
105  char rmTemp[PLEN] = "rm_";
106  char rmOutput[PLEN] = "rm_";
107  char rmtempLHpath[PLEN] = "rm_";
108  char rmWcPath[PLEN] = "rm_";
109  char rmWcOut[PLEN] = "rm_";
110  strcat(rmTemp,tempPath);
111  strcat(rmOutput,outputPath);
112  strcat(rmtempLHpath,tempLHpath);
113  strcat(rmWcPath,wcPath);
114  strcat(rmWcOut,outputWC);
115
116  // Read/write parameters sampled from GAMBIT
117  fp1 = fopen(tempLHpath,"r");
118  fp2 = fopen(tempPath,"w");
119
120  sprintf(newLH,"_1_%.10f\n",LH);
121  sprintf(newLHS,"_2_%.10f\n",LHS);
122  sprintf(newLS,"_4_%.10f\n",LS);
123  sprintf(newGX,"_5_%.10f\n",GX);
124  sprintf(newVS,"_7_%.10f\n",VS);
125  sprintf(newVH,"_8_%.10f\n",VH);
126
127  while (!feof(fp1))
128  {
129      // read line from input file
130      strcpy(str,"\0");
131      fgets(str,MAX,fp1);
132      if (!feof(fp1))
133      {
134          // step line by line
135          linectr++;
136          // if a line is the one specified, replace by the
137          // new, sampled param
138          if (linectr == lno1)
139          {
140              fprintf(fp2,"%s",newLH);
141          }
142          if (linectr == lno2)
143          {
144              fprintf(fp2,"%s",newLHS);
145          }
146          if (linectr == lno3)
147          {

```

```
147         fprintf(fp2, "%s ", newLS);
148     }
149     if (linectr == lno4)
150     {
151         fprintf(fp2, "%s ", newGX);
152     }
153     if (linectr == lno5)
154     {
155         fprintf(fp2, "%s ", newVS);
156     }
157     if (linectr == lno6)
158     {
159         fprintf(fp2, "%s ", newVH);
160     }
161     // if not, use the same as the original LesHouches
162     // file
163     if (linectr != lno1 && linectr != lno2 && linectr
164         != lno3 && linectr != lno4 && linectr != lno5
165         && linectr != lno6)
166     {
167         fprintf(fp2, "%s ", str);
168     }
169 }
170 fclose(fp1);
171 fclose(fp2);
172 // Temporary LesHouches is no longer needed
173 system(rmtempLHpath);
174 // Run SPheno
175 system(execCMD);
176 // Temporary input is no longer needed
177 system(rmTemp);
178 // Translate to EOS basis and run down the WCs to the b-
179 // physics scale.
180 // This function prints the WCs in the new basis to a new
181 // file.
182 system(execTranslate);
183 // SPheno output is no longer needed
184 system(rmOutput);
185 system(rmWcPath);
```

```
188
189 FILE *fp3;
190
191 // Extract WC's from the output
192
193 fp3 = fopen(outputWC, "r");
194
195 char line[256];
196 char templine[256];
197 char tempC[50];
198 double C1, C2, C3, C4, C5, C6;
199 double ReC7, ImC7, ReC7p, ImC7p;
200 double ReC8, ReC8p;
201 double ReC9, ImC9, ReC9p, ImC9p;
202 double ReC10, ImC10, ReC10p, ImC10p;
203 double ReCQ1, ImCQ1, ReCQ1p, ImCQ1p;
204 double ReCQ2, ImCQ2, ReCQ2p, ImCQ2p;
205 int i = 0;
206 while (fgets(line, sizeof(line), fp3))
207     {
208         i++;
209         if (i == 1)
210             {
211                 strcpy(templine, line);
212                 sscanf(templine, "%*s_%" , tempC);
213                 C1 = atof(tempC);
214             }
215         if (i == 2)
216             {
217                 strcpy(templine, line);
218                 sscanf(templine, "%*s_%" , tempC);
219                 C2 = atof(tempC);
220             }
221         if (i == 3)
222             {
223                 strcpy(templine, line);
224                 sscanf(templine, "%*s_%" , tempC);
225                 C3 = atof(tempC);
226             }
227         if (i == 4)
228             {
229                 strcpy(templine, line);
230                 sscanf(templine, "%*s_%" , tempC);
231                 C4 = atof(tempC);
232             }
233         if (i == 5)
```

```
234     {
235         strcpy(templine, line);
236         sscanf(templine, "%*s_%" ,tempC);
237         C5 = atof(tempC);
238     }
239     if (i == 6)
240     {
241         strcpy(templine, line);
242         sscanf(templine, "%*s_%" ,tempC);
243         C6 = atof(tempC);
244     }
245     if (i == 7)
246     {
247         strcpy(templine, line);
248         sscanf(templine, "%*s_%" ,tempC);
249         ReC7 = atof(tempC);
250     }
251     if (i == 8)
252     {
253         strcpy(templine, line);
254         sscanf(templine, "%*s_%" ,tempC);
255         ImC7 = atof(tempC);
256     }
257     if (i == 9)
258     {
259         strcpy(templine, line);
260         sscanf(templine, "%*s_%" ,tempC);
261         ReC7p = atof(tempC);
262     }
263     if (i == 10)
264     {
265         strcpy(templine, line);
266         sscanf(templine, "%*s_%" ,tempC);
267         ImC7p = atof(tempC);
268     }
269     if (i == 11)
270     {
271         strcpy(templine, line);
272         sscanf(templine, "%*s_%" ,tempC);
273         ReC8 = atof(tempC);
274     }
275     if (i == 12)
276     {
277         strcpy(templine, line);
278         sscanf(templine, "%*s_%" ,tempC);
279         ReC8p = atof(tempC);
```

```
280     }
281     if (i == 13)
282     {
283         strcpy(templine, line);
284         sscanf(templine, "%*s_%" ,tempC);
285         ReC9 = atof(tempC);
286     }
287     if (i == 14)
288     {
289         strcpy(templine, line);
290         sscanf(templine, "%*s_%" ,tempC);
291         ImC9 = atof(tempC);
292     }
293     if (i == 15)
294     {
295         strcpy(templine, line);
296         sscanf(templine, "%*s_%" ,tempC);
297         ReC9p = atof(tempC);
298     }
299     if (i == 16)
300     {
301         strcpy(templine, line);
302         sscanf(templine, "%*s_%" ,tempC);
303         ImC9p = atof(tempC);
304     }
305     if (i == 17)
306     {
307         strcpy(templine, line);
308         sscanf(templine, "%*s_%" ,tempC);
309         ReC10 = atof(tempC);
310     }
311     if (i == 18)
312     {
313         strcpy(templine, line);
314         sscanf(templine, "%*s_%" ,tempC);
315         ImC10 = atof(tempC);
316     }
317     if (i == 19)
318     {
319         strcpy(templine, line);
320         sscanf(templine, "%*s_%" ,tempC);
321         ReC10p = atof(tempC);
322     }
323     if (i == 20)
324     {
325         strcpy(templine, line);
```

```
326     sscanf(templine, "%*s_%" ,tempC);
327     ImC10p = atof(tempC);
328 }
329     if (i == 21)
330 {
331     strcpy(templine, line);
332     sscanf(templine, "%*s_%" ,tempC);
333     ReCQ1 = atof(tempC);
334 }
335     if (i == 22)
336 {
337     strcpy(templine, line);
338     sscanf(templine, "%*s_%" ,tempC);
339     ImCQ1 = atof(tempC);
340 }
341     if (i == 23)
342 {
343     strcpy(templine, line);
344     sscanf(templine, "%*s_%" ,tempC);
345     ReCQ1p = atof(tempC);
346 }
347     if (i == 24)
348 {
349     strcpy(templine, line);
350     sscanf(templine, "%*s_%" ,tempC);
351     ImCQ1p = atof(tempC);
352 }
353     if (i == 25)
354 {
355     strcpy(templine, line);
356     sscanf(templine, "%*s_%" ,tempC);
357     ReCQ2 = atof(tempC);
358 }
359     if (i == 26)
360 {
361     strcpy(templine, line);
362     sscanf(templine, "%*s_%" ,tempC);
363     ImCQ2 = atof(tempC);
364 }
365     if (i == 27)
366 {
367     strcpy(templine, line);
368     sscanf(templine, "%*s_%" ,tempC);
369     ReCQ2p = atof(tempC);
370 }
371     if (i == 28)
```

```

372     {
373         strcpy(templine, line);
374         sscanf(templine, "%*s %s", tempC);
375         ImCQ2p = atof(tempC);
376     }
377 }
378 fclose(fp3);
379
380 // The translated WC file is no longer needed
381 system("rmWcOut");
382
383 // adjust the basis to FlavBit conventions
384
385 double mB = 4180; // B-quark bar mass from PDG
386 // . unit: MeV
387 double mE = 0.5109989461; // electron mass from PDG. unit:
388 // MeV
389 double ratio = mB/mE;
390 ReCQ1 = ReCQ1*ratio;
391 ReCQ2 = ReCQ2*ratio;
392
393 printf("The Wilson coefficients passed onto parent is:\n")
394 ;
395 printf("%.30f\n", ReC7);
396 printf("%.30f\n", ReC9);
397 printf("%.30f\n", ReC10);
398 printf("%.30f\n", ReCQ1);
399 printf("%.30f\n", ReCQ2);
400
401 parentparams.setValue("Re_DeltaC7", ReC7);
402 parentparams.setValue("Re_DeltaC9", ReC9);
403 parentparams.setValue("Re_DeltaC10", ReC10);
404 parentparams.setValue("Re_DeltaCQ1", ReCQ1);
405 parentparams.setValue("Re_DeltaCQ2", ReCQ2);
406 }
407
408 #undef PARENT
409 #undef MODEL
410 #undef MAX
411 #undef STRPAR
412 #undef PLEN

```

C.3.3 LLrun.yaml

A sample YAML file runnable by GAMBIT using the WCVectorDM model. The path on line 168 need to be set according to the users conventions. Based on the WC.yaml example included in GAMBIT.

```

1 #####
2 ## GAMBIT configuration for a vectorial dark matter
3 ## model VDM
4 ## Uses likelihood constraints from flavour physics
5 ## observables only, without nuisance parameters.
6 #####
7
8
9 Parameters:
10
11   StandardModel_SLHA2:
12     alphaS      : 1.18500000E-01 #  $\alpha_s(m_Z)^{MSbar}$ 
13     mBmB       : 4.18000000E+00 #  $mb(mb)^{MSbar}$ 
14     alphainv   : 1.27940010E+02 #  $\alpha^{-1}(m_Z)^{MSbar}$ 
15     mT         : 1.73340000E+02 #  $m_{top}(pole)$ 
16     GF         : 1.16637870E-05 #  $G_{Fermi}$ 
17     mZ         : 9.11876000E+01 #  $m_Z(pole)$ 
18     mTau       : 1.77682000E+00 #  $m_{\tau}(pole)$ 
19     mNu3       : 0 #  $m_{\nu 3}(pole)$ 
20     mD         : 4.80000000E-03 #  $m_D(2 GeV)^{MSbar}$ 
21     mU         : 2.30000000E-03 #  $m_U(2 GeV)^{MSbar}$ 
22     mS         : 9.50000000E-02 #  $m_S(2 GeV)^{MSbar}$ 
23     mCmC      : 1.27500000E+00 #  $m_C(mc)^{MSbar}$ 
24     mE         : 5.10998928E-04 #  $m_{electron}(pole)$ 
25     mMu       : 1.05658372E-01 #  $m_{\mu}(pole)$ 
26     mNu1      : 0 #  $m_{\nu 1}(pole)$ 
27     mNu2      : 0 #  $m_{\nu 2}(pole)$ 
28     CKM_lambda : 0.22537 # Wolfenstein  $|\lambda|$ 
29     CKM_A      : 0.814 # Wolfenstein  $A$ 
30     CKM_rhobar : 0.117 # Wolfenstein  $|\bar{\rho}|$ 
31     CKM_etabar : 0.353 # Wolfenstein  $|\bar{\eta}|$ 
32     theta12    : 0.58376 # solar angle
33     theta23    : 0.76958 # atmospheric mixing angle
34     theta13    : 0.15495 # reactor angle
35     delta13    : 0 # Dirac CP-violating phase
36     alpha1     : 0 # first Majorana CP-
        violating phase
37     alpha2     : 0 # second CP-violating
        Majorana phase
38
39   StandardModel_Higgs:

```

```
40     mH: 125.09
41
42     WCVectorDM:
43     M1:
44         range: [0.01,70]
45         prior_type: log
46     M2: 125.09
47     MV:
48         fixed_value: 30
49     sinTheta:
50         range: [0.001,1]
51         prior_type: log
52     vH: 246.22
53     gX:
54         fixed_value: 0.1
55
56     Priors:
57
58     # All priors are simple, so specified in Parameters
59     # section
60
61     Printer:
62
63     printer: hdf5
64
65     options:
66         output_file: "LLrun1-multinest.hdf5"
67         group: "/WCVectorDM"
68
69     Scanner:
70
71
72     use_scanner: multinest
73
74     scanners:
75
76     multinest:
77         plugin: multinest
78         like: LogLike
79         nlive: 20000
80         tol: 1e-3
81
82     de:
83         plugin: diver
84         like: LogLike
```

C. Source code

```
85     NP: 20000
86     convthresh: 1e-4
87
88     square_grid:
89     plugin: square_grid
90     like: LogLike
91     grid_pts: 20
92
93
94 ObsLikes:
95
96     # Likelihoods
97     - purpose:      LogLike
98     capability: b2ll_LL
99
100    purpose:      LogLike
101    capability: b2sll_LL
102
103    purpose:      LogLike
104    capability: b2sgamma_LL
105
106    # Observables
107    purpose:      Observable
108    capability: bsgamma
109
110    - purpose:      Observable
111    capability: Bsmumu_untag
112
113    - purpose:      Observable
114    capability: Bmumu
115
116    - purpose:      Observable
117    capability: Bsee_untag
118
119    purpose:      Observable
120    capability: BKstarmumu_11_25
121
122    purpose:      Observable
123    capability: BKstarmumu_25_40
124
125    purpose:      Observable
126    capability: BKstarmumu_40_60
127
128    purpose:      Observable
129    capability: BKstarmumu_60_80
130
```

```
131  # purpose:    Observable
132  # capability: BKstarmumu_15_17
133
134  # purpose:    Observable
135  # capability: BKstarmumu_17_19
136
137
138 Rules:
139
140  # Use SuperIso instead of FeynHiggs for b->sgamma
141  # capability: bsgamma
142  # function: SI_bsgamma
143
144  # Use SuperIso instead of FeynHiggs for B_s->mumu
145  - capability: Bsmumu_untag
146    function: SI_Bsmumu_untag
147  - capability: Bsee_untag
148    function: SI_Bsee_untag
149
150
151 Logger:
152
153   redirection:
154     [Debug]    : "debug.log"
155     [Default]  : "default.log"
156     [FlavBit] : "FlavBit.log"
157
158
159 KeyValues:
160
161   dependency_resolution:
162     prefer_model_specific_functions: true
163
164   likelihood:
165     model_invalid_for_lnlake_below: -5e5
166     model_invalid_for_lnlake_below_alt: -1e5
167
168   default_output_path: ${TMPDIR}/LLrun1-multinest
169
170   debug: false
```

DEPARTMENT OF PHYSICS
CHALMERS UNIVERSITY OF TECHNOLOGY
Gothenburg, Sweden
www.chalmers.se



CHALMERS
UNIVERSITY OF TECHNOLOGY